efficiently in vitro in coculture with OP9 stromal cells. Furthermore, mGS-derived hematopoietic cells engrafted in the BM of NOD/SCIDγc^{null} mice, although their chimeric rate was very low. We have also transplanted hematopoietic cells differentiated from mGS-derived Flk1$^+$ cells into lethally irradiated mice via tail vein, but found no significant number of donor cells in the PB or BM after transplantation (more than 30 transplanted mice, data not shown). mGS-derived cells were found in the recipient BM only when directly transplanted into the femoral BM of NOD/SCIDγc^{null} mice.

There may be several reasons why the mGS-derived Flk1$^+$ progeny only engraft upon direct injection into the marrow. It is known that emergence of hematopoiesis from ES cells in vitro mirrors the emergence of hematopoiesis in the murine embryos [26]. Considering this observation, hematopoietic cells derived from mGS and ES cells should have similar characteristics to hematopoietic cells in embryos during early–mid gestation. Yolk sac cells and para-aortic splanchnopleura cells as early as E9.0 engraft in sublethally conditioned neonatal mice, but not in adult BM [27,28]. These facts lead us to speculate that mGS-derived hematopoietic cells may be too immature to express homing receptors and thus failed to find the HSC niche in the adult BM when circulating. Indeed, very few mGS-derived cells expressed CXCR4, c-kit, or Sca-1 (Fig. 8C). Furthermore, the mGS-derived Flk1$^+$ progeny may fail to express high levels of human leukocyte antigen (HLA) and thus are trapped by host natural killer (NK) cells. However, NOD/SCIDγc^{null} mice have no NK cell activity [29,30] and are thus suitable for transplantation with embryonic HSCs that have just emerged from the aorta-gonado-mesonephros region at E10.5 [31]. Finally, we may have observed low chimerism due to the limited number of cells infused (1×10^5). Transplanting a larger number of cells might improve the chimerism. This limited proliferative ability of transplanted cells is similar to the behavior of human ES-derived cells transplanted in NOD/SCID mice [32].

It is interesting that donor mGS–derived hematopoietic cells that engrafted remained at the endosteal region, reported to be a niche for HSC, and that they were resident in the SP fraction 4 months after transplantation. However, these mGS-derived hematopoietic cells could not proliferate even after 5FU injection; a hematopoietic stress that normally recruits quiescent HSC into cycle and replenishment of the 5FU–depleted progenitor cell pool. In the secondary transplantation studies, as many as 30,000 to 40,000 cells were sorted from the BM of the primary recipients and injected into secondary recipient BM, and no donor cells were observed. While the most quiescent

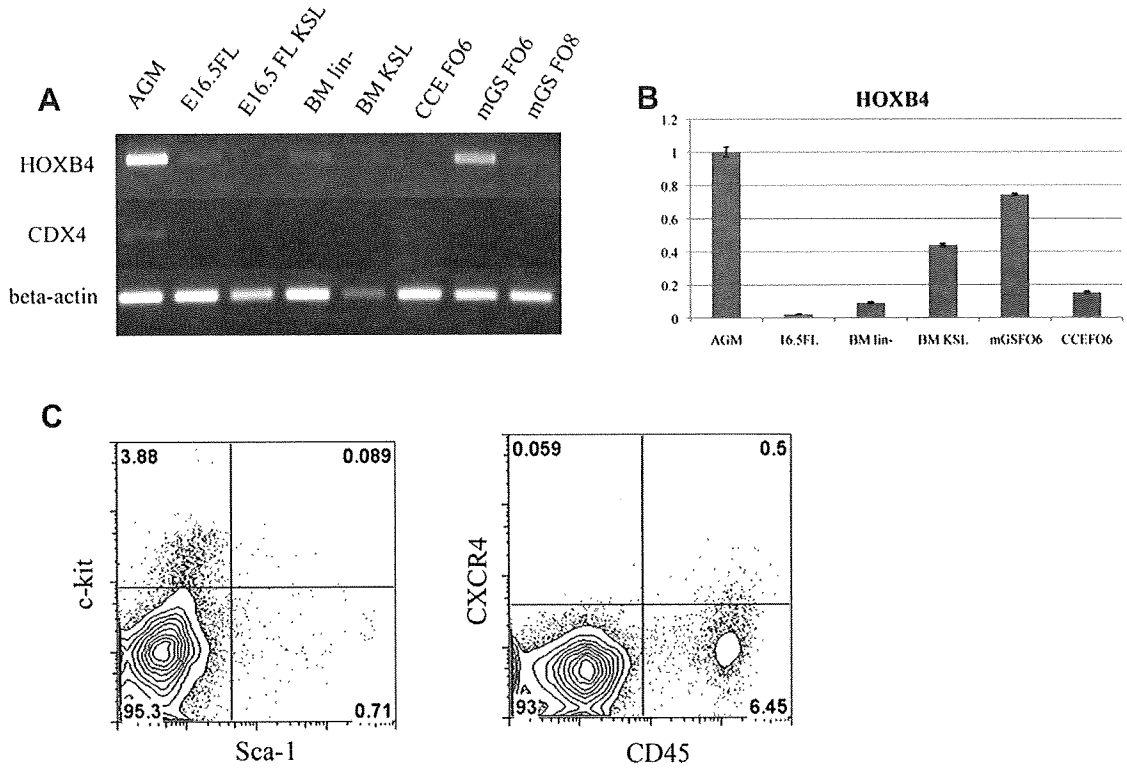

Figure 8. mGS–derived cells express HOXB4, but not CDX4 or CXCR4. RT-PCR for CDX4 and HOXB4 among various hematopoitic cells (**A**). KSL = c-kit$^+$Sca-1$^+$lineage$^-$ cells, BM lin$^-$ = bone marrow lineage-negative cells, FO6 = Flk1 culture on OP9 day 6, FO8 = Flk1 culture on OP9 day 8. Relative HOXB4 expression in the various hematopoitic cells (**B**). With AGM as a reference, the relative expressions of HOXB4 in each sample were follows; 16.5FL 0.02, BM lin$^-$ 0.09, BM KSL 0.43, mGS FO6 0.74, CCE FO6 0.15. c-kit, Sca-1, and CXCR4 expression on mGS-derived cells [(**C**) 6 days culture].

dormant HSCs may divide every 145 days, even dormant HSC can proliferate after 5FU injection [33]. Therefore, it is unlikely that our mGS-derived multipotent cells represent dormant HSCs.

We have also shown that mGS-derived Flk-1^+ cells could produce B- and T-lymphoid cells, as well as erythromyeloid cells, using OP9 and OP9-DL1 stromal cell line cocultures. These results were very similar to ES cell differentiation studies reported previously [12,22]. Thus, mGS cells have at least the same hematopoietic potential as ES cells in vitro and in vivo.

Wild-type ES cells fail to reconstitute mouse BM without prior genetic modification [1,2]. Considering that only CDX4- and HOX B4-expressing ES cells can engraft and proliferate in vivo, it might be possible that ES or mGS-derived hematopoietic cells originally lack the proliferation potential required for in vivo expansion following engraftment. Actually, our mGS-derived cells, as well as fetal liver and BM stem/progenitor cells, did not express CDX4 transcripts. On the other hand, mGS-derived cells did express HOXB4. Because mGS-derived cells could not expand in vivo in spite of higher HOXB4 expression than fetal liver and BM progenitors, lack of CXCR4 expression may be a primary reason for the low level of donor cell chimerism rather than lack of CDX4 expression, although the question of whether upregulating CDX4 expression may enhance repopulating ability of the transplanted mGS cells needs further study. Nevertheless, this is the first report that transplanted hematopoietic cells derived from ES-like cells (mGS or ES cells) may reside in a long-lived multipotent hematopoietic cell fraction in vivo.

Recently, multipotent germline stem cells have been established from adult mouse testis [34]. Multipotent adult germline stem cells display similar characteristics to ES cells, including contributions to various organs (even germline transmission) when injected into an early blastocyst. The multipotent adult GS cells possess an advantage over ES or embryonic germ cells because they can be stably established from the postnatal mouse. Establishing multipotent adult GS cells from human subjects should be feasible both technically and ethically. Indeed, pluripotent stem cells from adult human testis have been generated [35,36]. Additionally, induced pluripotent stem cells have been established from mouse and human somatic cells and upon differentiation induced pluripotent stem cell progeny appear to have the same potential as ES-derived cells [37–39]. Which cell source will ultimately prove most efficacious for human therapy remains fertile ground for future translational research.

Acknowledgments

This study was supported by grants for Scientific Research (S) (19109006) and Scientific Research (B) (18390298,20390296) from the Ministry of Education, Science, Technology, Sports and Culture of Japan (Tokyo, Japan), Uehara Memorial Foundation (Tokyo, Japan) and by the Riley Children's Foundation (Indianapolis, IN, USA).

Conflict of Interest Disclosure

No financial interests/relationships with financial interest relating to the topic of this article have been declared.

References

1. Kyba M, Perlingeiro RC, Daley GQ. HoxB4 confers definitive lymphoid-myeloid engraftment potential on embryonic stem cell and yolk sac hematopoietic progenitors. Cell. 2002;109:29–37.
2. Wang Y, Yates F, Naveiras O, Ernst P, Daley GQ. Embryonic stem cell-derived hematopoietic stem cells. Proc Natl Acad Sci U S A. 2005;102:19081–19086.
3. Kanatsu-Shinohara M, Inoue K, Lee J, et al. Generation of pluripotent stem cells from neonatal mouse testis. Cell. 2004;119:1001–1012.
4. Kennedy M, Firpo M, Choi K, et al. A common precursor for primitive erythropoiesis and definitive haematopoiesis. Nature. 1997;386:488–493.
5. Kataoka H, Takakura N, Nishikawa S, et al. Expressions of PDGF receptor alpha, c-Kit and Flk1 genes clustering in mouse chromosome 5 define distinct subsets of nascent mesodermal cells. Dev Growth Differ. 1997;39:729–740.
6. Shalaby F, Rossant J, Yamaguchi TP, et al. Failure of blood-island formation and vasculogenesis in Flk-1-deficient mice. Nature. 1995; 376:62–66.
7. Shalaby F, Ho J, Stanford WL, et al. A requirement for Flk1 in primitive and definitive hematopoiesis and vasculogenesis. Cell. 1997;89: 981–990.
8. Nishikawa SI, Nishikawa S, Hirashima M, Matsuyoshi N, Kodama H. Progressive lineage analysis by cell sorting and culture identifies FLK1+VE-cadherin+ cells at a diverging point of endothelial and hemopoietic lineages. Development. 1998;125:1747–1757.
9. Nakano T, Kodama H, Honjo T. Generation of lymphohematopoietic cells from embryonic stem cells in culture. Science. 1994;265:1098–1101.
10. Nishikawa SI, Nishikawa S, Kawamoto H, et al. In vitro generation of lymphohematopoietic cells from endothelial cells purified from murine embryos. Immunity. 1998;8:761–769.
11. Iida M, Heike T, Yoshimoto M, Baba S, Doi H, Nakahata T. Identification of cardiac stem cells with FLK1, CD31, and VE-cadherin expression during embryonic stem cell differentiation. FASEB J. 2005;19:371–378.
12. Schmitt TM, de Pooter RF, Gronski MA, Cho SK, Ohashi PS, Zuniga-Pflucker JC. Induction of T cell development and establishment of T cell competence from embryonic stem cells differentiated in vitro. Nat Immunol. 2004;5:410–417.
13. Nakahata T, Ogawa M. Identification in culture of a class of hemopoietic colony-forming units with extensive capability to self-renew and generate multipotential hemopoietic colonies. Proc Natl Acad Sci U S A. 1982;79:3843–3847.
14. Nakahata T, Ogawa M. Hemopoietic colony-forming cells in umbilical cord blood with extensive capability to generate mono- and multipotential hemopoietic progenitors. J Clin Invest. 1982;70:1324–1328.
15. Miwa Y, Atsumi T, Imai N, Ikawa Y. Primitive erythropoiesis of mouse teratocarcinoma stem cells PCC3/A/1 in serum-free medium. Development. 1991;111:543–549.
16. Goodell MA, Brose K, Paradis G, Conner AS, Mulligan RC. Isolation and functional properties of murine hematopoietic stem cells that are replicating in vivo. J Exp Med. 1996;183:1797–1806.
17. Tsuchiya A, Heike T, Fujino H, et al. Long-term extensive expansion of mouse hepatic stem/progenitor cells in a novel serum-free culture system. Gastroenterology. 2005;128:2089–2104.

18. Nagato M, Heike T, Kato T, et al. Prospective characterization of neural stem cells by flow cytometry analysis using a combination of surface markers. J Neurosci Res. 2005;80:456–466.
19. Yoshimoto M, Chang H, Shiota M, et al. Two different roles of purified CD45+c-Kit+Sca-1+Lin- cells after transplantation in muscles. Stem Cells. 2005;23:610–618.
20. Umeda K, Heike T, Yoshimoto M, et al. Development of primitive and definitive hematopoiesis from nonhuman primate embryonic stem cells in vitro. Development. 2004;131:1869–1879.
21. Umeda K, Heike T, Yoshimoto M, et al. Identification and characterization of hemoangiogenic progenitors during cynomolgus monkey embryonic stem cell differentiation. Stem Cells. 2006;24:1348–1358.
22. Fujimoto T, Ogawa M, Minegishi N, et al. Step-wise divergence of primitive and definitive haematopoietic and endothelial cell lineages during embryonic stem cell differentiation. Genes Cells. 2001;6: 1113–1127.
23. Yoshimoto M, Shinohara T, Heike T, Shiota M, Kanatsu-Shinohara M, Nakahata T. Direct visualization of transplanted hematopoietic cell reconstitution in intact mouse organs indicates the presence of a niche. Exp Hematol. 2003;31:733–740.
24. Arai F, Hirao A, Ohmura M, et al. Tie2/angiopoietin-1 signaling regulates hematopoietic stem cell quiescence in the bone marrow niche. Cell. 2004;118:149–161.
25. Nilsson SK, Johnston HM, Coverdale JA. Spatial localization of transplanted hemopoietic stem cells: inferences for the localization of stem cell niches. Blood. 2001;97:2293–2299.
26. Choi K. The hemangioblast: a common progenitor of hematopoietic and endothelial cells. J Hematother Stem Cell Res. 2002;11:91–101.
27. Yoder MC, Hiatt K, Dutt P, Mukherjee P, Bodine DM, Orlic D. Characterization of definitive lymphohematopoietic stem cells in the day 9 murine yolk sac. Immunity. 1997;7:335–344.
28. Yoder MC, Hiatt K, Mukherjee P. In vivo repopulating hematopoietic stem cells are present in the murine yolk sac at day 9.0 postcoitus. Proc Natl Acad Sci U S A. 1997;94:6776–6780.
29. Ito M, Hiramatsu H, Kobayashi K, et al. NOD/SCID/gamma(c)(null) mouse: an excellent recipient mouse model for engraftment of human cells. Blood. 2002;100:3175–3182.
30. Hiramatsu H, Nishikomori R, Heike T, et al. Complete reconstitution of human lymphocytes from cord blood CD34+ cells using the NOD/SCID/gammacnull mice model. Blood. 2003;102: 873–880.
31. Cumano A, Ferraz JC, Klaine M, Di Santo JP, Godin I. Intraembryonic, but not yolk sac hematopoietic precursors, isolated before circulation, provide long-term multilineage reconstitution. Immunity. 2001;15:477–485.
32. Wang L, Menendez P, Shojaei F, et al. Generation of hematopoietic repopulating cells from human embryonic stem cells independent of ectopic HOXB4 expression. J Exp Med. 2005;201:1603–1614.
33. Wilson A, Laurenti E, Oser G, et al. Hematopoietic stem cells reversibly switch from dormancy to self-renewal during homeostasis and repair. Cell. 2008;135:1118–1129.
34. Guan K, Nayernia K, Maier LS, et al. Pluripotency of spermatogonial stem cells from adult mouse testis. Nature. 2006;440: 1199–1203.
35. Conrad S, Renninger M, Hennenlotter J, et al. Generation of pluripotent stem cells from adult human testis. Nature. 2008;456:344–349.
36. Kossack N, Meneses J, Shefi S, et al. Isolation and characterization of pluripotent human spermatogonial stem cell-derived cells. Stem Cells. 2009;27:138–149.
37. Takahashi K, Tanabe K, Ohnuki M, et al. Induction of pluripotent stem cells from adult human fibroblasts by defined factors. Cell. 2007;131: 861–872.
38. Takahashi K, Yamanaka S. Induction of pluripotent stem cells from mouse embryonic and adult fibroblast cultures by defined factors. Cell. 2006;126:663–676.
39. Wernig M, Meissner A, Foreman R, et al. In vitro reprogramming of fibroblasts into a pluripotent ES-cell-like state. Nature. 2007;448: 318–324.

TABLE 2 Details of response to sequential treatments where applicable ($n = 10$)

No.	Severity of disease	First treatment		Second treatment		Third treatment	
1	Severe	Amlodopine	×	Nifedipine	√	–	–
2	Moderate	Amlodopine	×	GTN	×	–	–
3	Moderate	Amlodopine	×	GTN	×	–	–
4	Severe	Nifedipine	×	Amlodopine	×	–	–
5	Severe	Nifedipine	×	Amlodopine	×	GTN	√
6	Moderate	Nifedipine	×	GTN	×	–	
7	Severe	GTN	×	Amlodopine	×	Nifedipine	√
8	Moderate	Nifedipine	×	GTN	√	–	–
9	Severe	Amlodopine	×	Nifedipine	×	GTN	×
10	Moderate	Amlodopine	√	GTN	√	–	–

×: no response/inadequate response; √: response.

Overall, GTN patches were effective in 55% of the treated patients. Efficacy was better than that of nifedipine and amlodipine (33 *vs* 25% response rate, respectively), but small numbers and retrospective analysis does not allow statistical comparison. Response was similar in primary and secondary RP. Children with severe RP had a better response to nifedipine and amlodopine than children with moderate disease. The sub-group with severe disease was more likely to be using a disease-modifying drug, which may have had an impact. However, numbers are too small for any conclusion to be drawn from this.

Application of GTN patches allows removal if adverse events occur. Together with absence of tablets, this may make treatment with GTN attractive in paediatric practice. All patients received Deponit GTN patches. Alternative brands may not have adequate skin adhesion when cut into quarters for this off-license use.

GTN patches, nifedipine and amlodipine offer symptomatic relief for patients with moderate primary/secondary RP. Further studies, including head-to-head trials, are needed to determine if one agent is superior. Meanwhile, GTN patches offer an alternative to oral calcium channel blockers for symptomatic relief of paediatric RP.

Rheumatology key message

- GTN patches are an efficacious treatment option in paediatric RP.

Disclosure statement: The authors have declared no conflicts of interest.

Kapil Gargh[1], Eileen M. Baildam[1], Gavin A. Cleary[1], Michael W. Beresford[1] and Liza J. McCann[1]

[1]*Department of Paediatric Rheumatology, Alder Hey Children's NHS Foundation Trust, Liverpool, UK*
Accepted 20 August 2009
Correspondence to: Liza McCann, Department of Paediatric Rheumatology, Alder Hey Children's NHS Foundation Trust, Eaton Road, Liverpool, L12 2AP, UK.
E-mail: liza.mccann@alderhey.nhs.uk

References

1 Anderson ME, Moore TL, Hollis S, Jayson MIV, King TA, Herrick AL. Digital vascular response to topical glyceryl trinitrate, as measured by laser Doppler imaging, in primary Raynaud's phenomenon and systemic sclerosis. Rheumatology 2002;41:324–28.

2 Franks AG Jr. Topical glyceryl trinitrate as adjunctive treatment in Raynaud's disease. Lancet 1982;1:76–7.

3 Teh LS, Mannig J, Moore T, Tully MP, O'Reilly D, Jayson MIV. Sustained-release transdermal glyceryl trinitrate patches as a treatment for primary and secondary Raynaud's phenomenon. Br J Rheumatol 1995; 34:636–41.

4 Nigrovic PA, Fuhlbrigge RC, Sundel RP. Raynaud's phenomenon in children: a retrospective review of 123 patients. Pediatrics 2003;111:715–21.

5 Coppock JS, Hardman JM, Bacon PA, Woods KL, Kendall MJ. Objective relief of vasospasm by glyceryl trinitrate in secondary Raynaud's phenomenon. Postgrad Med J 1986;62:8–15.

Rheumatology 2010;49:194–196
doi:10.1093/rheumatology/kep315
Advance Access publication 23 October 2009

A case of early-onset sarcoidosis with a six-base deletion in the *NOD2* gene

SIR, We present the first case of early-onset sarcoidosis (EOS, MIM no. 609464) with a six-base deletion in the *NOD2* gene, resulting in the replacement of one amino acid and the deletion of two additional amino acids. All previous mutations reported for EOS and Blau syndrome (BS, MIM no. 186580) were single-base substitutions that resulted in the replacement of a single amino acid [1–3].

The patient was a Japanese male born after an uncomplicated pregnancy and delivery. His family had no symptoms of skin lesions, arthritis or uveitis. At 5 years of age, he was diagnosed with bilateral severe uveitis. He became blind in both eyes during adolescence. He had swollen ankles without pain during childhood,

and developed arthritis in his both knees and ankles at 15 years of age. At 30 years, a skin rash had developed on his extremities after his first BCG vaccination. The skin lesions were scaly erythematous plaques with multiple lichenoid papules and some pigmentation. At the same age, camptodactyly without obvious synovial cysts of the hands was observed, and the deformity in all fingers developed by 35 years. At 41 years, he had low-grade fever for 1 year. He had no pulmonary lesions. His laboratory investigations showed normal white blood cell count, mildly elevated CRP (1.0 mg/dl) and ESR (20 mm/h). A skin biopsy from his left forearm revealed non-caseating granulomas without lymphocyte infiltration. There were no indications of infection by *Mycobacterium*.

The clinical symptoms and pathological findings on the biopsied skin indicated that the patient suffered from EOS. It has been reported that EOS and BS have a common genetic aetiology due to mutations in the *NOD2* gene that cause constitutive Nuclear Factor (NF)-κB activation [4, 5]. Thus we analysed the *NOD2* gene from the patient to look for mutations that might correlate with the pathology of EOS. A written informed consent was obtained from the patient and his families, according to the protocol of the institutional review board of Kyoto University Hospital and in accordance with the Declaration of Helsinki. Genomic sequencing analysis of the patient's *NOD2* gene showed the presence of a heterozygous deletion of six bases in exon 4, which resulted in c.1493_1498delAACTGT, p.E498V, 499–500del (Fig. 1A). The mutation was novel and was not identified in 100 normal controls. A genome alignment of *NOD2* among several species showed that E498, L499 and L500 are conserved from zebrafish to human (Fig. 1B). These data strongly suggested that the identified deletion of six bases in the *NOD2* gene is not a single nucleotide polymorphism (SNP), but is probably responsible for EOS in the patient.

Previous studies report that *NOD2* mutations causing EOS/BS show constitutive activation of NF-κB [6–8]. Therefore, we investigated the level of NF-κB activity associated with the new mutation identified here. First, we confirmed the level of mRNA expression of the mutated allele by subcloning analysis of *NOD2*-cDNA, which showed that the mutated allele was expressed as well as the wild type allele (data not shown). We then evaluated the ability of the *NOD2* mutant to constitutively activate NF-κB by using an *in vitro* reporter system in HEK293T cells transfected with both *NOD2* mutants and NF-κB reporter plasmids (Fig. 1C). The deletion mutant demonstrated almost five times more NF-κB activity than wild type without muramyl dipeptide (MDP) stimulation. Western blot analysis confirmed that NOD2 mutant protein expression was similar to that of wild type (Fig. 1C). Thus, like other mutations of *NOD2* identified previously, the deletion mutant identified here also showed constitutive activation of NF-κB.

The mechanism underlying EOS/BS has not been totally understood, although two pathways downstream from *NOD2* have been identified: NF-κB activation through receptor-interacting protein (RIP) like interacting caspase-like apoptosis regulatory protein kinase (RICK) and MAP kinase activation through the caspase recruitment domain 9 (CARD9) [9]. We previously tested 10 *NOD2* missense mutations that have been identified in our cohort of EOS/BS patients in Japan, and all of them demonstrated constitutive activation of NF-κB [3]. By analysing this newly identified deletion mutant, we have further confirmed the importance of constitutive activation of NF-κB by mutated *NOD2* for the pathogenesis of EOS/BS. We would like to emphasize the

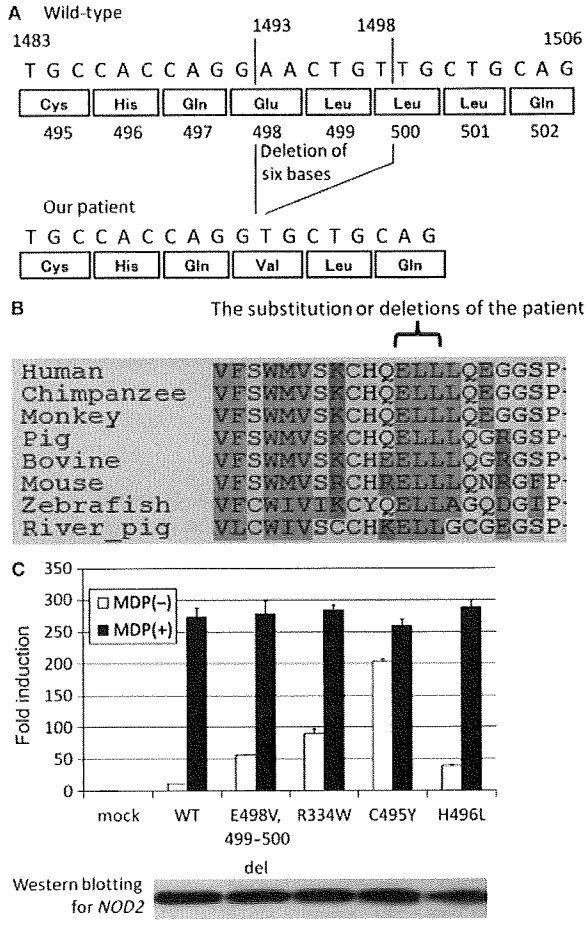

FIG. 1 (**A**) Summary of the mutations identified in our patient. (**B**) NOD2 protein alignment among different species on the mutated amino acids. (**C**) NF-κB reporter assay using the *NOD2* deletion mutant. *In vitro* NF-κB reporter assays were performed as previously described [1, 3, 6, 7]. Mock vector, wild type *NOD2* (WT) and three *NOD2* variants (R334W, C495Y, H496L) derived from EOS/BS patients, were used as controls. Values represent the mean of normalized data (mock without MDP = 1) of triplicate cultures, and error bars indicate S.D. Shown is one representative result of three independent experiments. Protein expression levels of *NOD2* mutants analysed by western blotting are shown in the bottom panel.

usefulness of the NF-κB reporter assay with mutant *NOD2* for observing its role in EOS/BS, although the MAP kinase activation pathway and other possible pathways need to be evaluated to more completely understand the pathogenesis of the *NOD2* mutation in EOS/BS.

We have identified the first deletion mutation in the *NOD2* gene responsible for EOS/BS, and the mutant showed constitutive activation of NF-κB, which is one of the key features that lead to the pathogenesis of EOS/BS.

Rheumatology key message

- A six-base deletion in *NOD2* gene causes EOS.

Acknowledgement

This work was carried out at Department of Pediatrics, Kyoto University Graduate School of Medicine, Kyoto, Japan.

Funding: This work was supported by grants from the Japanese Ministry of Education, Culture, Sports, Science and Technology and grants from the Japanese Ministry of Health, Labor and Welfare.

Disclosure statement: The authors have declared no conflicts of interest.

Hidemasa Sakai[1], Shusaku Ito[2], Ryuta Nishikomori[1], Yuuki Takaoka[1], Tomoki Kawai[1], Megumu Saito[1], Ikuo Okafuji[3], Takahiro Yasumi[1], Toshio Heike[1] and Tatsutoshi Nakahata[1]

[1]*Department of Pediatrics, Kyoto University Graduate School of Medicine, Kyoto,* [2]*Department of Dermatology, Hitachi General Hospital, Hitachi and* [3]*Department of Pediatrics, Kobe City Medical Center General Hospital, Kobe, Japan*
Accepted 27 August 2009
Correspondence to: Ryuta Nishikomori, Department of Pediatrics, Kyoto University Graduate School of Medicine, 54 Kawahara-cho, Shogoin, Sakyo-ku, Kyoto 606-8507, Japan. E-mail: rnishiko@kuhp.kyoto-u.ac.jp

References

1 Rosé CD, Wouters CH, Meiorin S *et al.* Pediatric granulomatous arthritis: an international registry. Arthritis Rheum 2006;54:3337–44.

2 Aróstegui JI, Arnal C, Merino R *et al. NOD2* gene-associated pediatric granulomatous arthritis: clinical diversity, novel and recurrent mutations, and evidence of clinical improvement with interleukin-1 blockade in a Spanish cohort. Arthritis Rheum 2007;56:3805–13.

3 Okafuji I, Nishikomori R, Kanazawa N *et al.* Role of the *NOD2* genotype in the clinical phenotype of Blau syndrome and Early-onset sarcoidosis. Arthritis Rheum 2009;60:242–50.

4 Kanazawa N, Okafuji I, Kambe N *et al.* Early-onset sarcoidosis and *CARD15* mutations with constitutive nuclear factor κB activation: common genetic etiology with Blau syndrome. Blood 2005;105:1195–97.

5 Rosé CD, Doyle TM, McIlvain-Simpson G *et al.* Blau syndrome mutation of *CARD15/NOD2* in sporadic early onset granulomatous arthritis. J Rheumatol 2005;32:373–5.

6 Chamaillard M, Philpott D, Girardin SE *et al.* Gene-environment interaction modulated by allelic heterogeneity in inflammatory diseases. Proc Natl Acad Sci USA 2003;100:3455–60.

7 Becker ML, Rosé CD. Blau syndrome and related genetic disorders causing childhood arthritis. Curr Rheumatol Rep 2005;7:427–33.

8 Kambe N, Nishikomori R, Kanazawa N. The cytosolic pattern-recognition receptor NOD2 and inflammatory granulomatous disorders. J Dermatol Sci 2005;39:71–80.

9 Hsu YM, Zhang Y, You Y *et al.* The adaptor protein CARD9 is required for innate immune responses to intracellular pathogens. Nat Immunol 2007;8:198–205.

Rheumatology 2010;49:196–197
doi:10.1093/rheumatology/kep330
Advance Access publication 25 October 2009

Comment on: Hepatotoxicity rates do not differ in patients with rheumatoid arthritis and psoriasis treated with methotrexate

SIR, We read with interest the recent article by Amital *et al.* [1] that compared hepatotoxicity rates in PsA and RA patients treated with MTX based on the evaluation of standard liver function tests. The authors conclude that the incidence of hepatotoxicity does not differ between the two disease groups after adjusting for the cumulative dose of MTX.

Several studies in MTX-treated psoriasis patients have reported that isolated abnormalities of liver enzymes (i.e. alkaline phosphatase, aspartate aminotransferase and alanine aminotransferase) were poor predictors of the severity of liver histopathology. The authors state that the combined sensitivity of aspartate aminotransferase, alanine aminotransferase and bilirubin for detecting an abnormal liver biopsy has been rated at 0.86 based on a previous study [2]. This figure implies that 14% of those with normal liver function tests will have undetected hepatic disease. Larger studies have suggested that 30–50% of the psoriasis patients on MTX have normal standard liver function test results despite histology showing fibrosis and cirrhosis [3]. The lack of correlation between liver enzymes and hepatic fibrosis and cirrhosis has been the major factor leading to the recommendation that liver biopsies be done to monitor potential hepatotoxicity. In this study, the liver function tests were performed with varying frequency which could allow abnormal liver function tests to be missed. The authors acknowledge that the rates of other hepatotoxic agents such as alcohol use and the occurrence of other hepatic comorbidities were not known. We believe that these are significant confounding variables, which make the interpretation of the results of this study difficult. The British Association of Dermatologists recommends serial monitoring

The endothelial antigen ESAM marks primitive hematopoietic progenitors throughout life in mice

Takafumi Yokota,[1] Kenji Oritani,[1] Stefan Butz,[2] Koichi Kokame,[3] Paul W. Kincade,[4] Toshiyuki Miyata,[3] Dietmar Vestweber,[2] and Yuzuru Kanakura[1]

[1]Department of Hematology and Oncology, Osaka University Graduate School of Medicine, Suita, Japan; [2]Department of Vascular Cell Biology, Max-Planck-Institute for Molecular Biomedicine, Münster, Germany; [3]National Cardiovascular Center Research Institute, Osaka, Japan; and [4]Immunobiology and Cancer Program, Oklahoma Medical Research Foundation, Oklahoma City

Although recent advances have enabled hematopoietic stem cells (HSCs) to be enriched to near purity, more information about their characteristics will improve our understanding of their development and stage-related functions. Here, using microarray technology, we identified endothelial cell-selective adhesion molecule (ESAM) as a novel marker for murine HSCs in fetal liver. *Esam* was expressed at high levels within a Rag1$^-$ c-kit^{Hi} Sca1$^+$ HSC-enriched fraction, but sharply down-regulated with activation of the Rag1 locus, a valid marker for the most primitive lymphoid progenitors in E14.5 liver. The HSC-enriched fraction could be subdivided into 2 on the basis of ESAM levels. Among endothelial antigens on hematopoietic progenitors, ESAM expression showed intimate correlation with HSC activity. The ESAM^{Hi} population was highly enriched for multipotent myeloid-erythroid progenitors and primitive progenitors with lymphopoietic activity, and exclusively reconstituted long-term lymphohematopoiesis in lethally irradiated recipients. Tie2$^+$ c-kit$^+$ lymphohematopoietic cells in the E9.5–10.5 aorta-gonad-mesonephros region also expressed high levels of ESAM. Furthermore, ESAM was detected on primitive hematopoietic progenitors in adult bone marrow. Interestingly, ESAM expression in the HSC-enriched fraction was up-regulated in aged mice. We conclude that ESAM marks HSC in murine fetal liver and will facilitate studies of hematopoiesis throughout life. (Blood. 2009;113:2914-2923)

Introduction

Hematopoietic stem cells (HSCs) are defined as cells with the capacity for self-renewal as well as differentiation into multilineage blood cells, maintaining the immune system throughout life. A large body of information exists about molecular mechanisms involved in maintaining their integrity, and many studies have attempted to identify unique markers associated with these extremely rare cells. In bone marrow of adult mice, the Lin$^-$ c-kit^{Hi} Sca1$^+$ CD34$^{-/Lo}$ Thy1.1^{Lo} subset is known to include HSCs with long-term repopulating capacity.[1] However, several of these parameters differ between strains of mice, change dramatically during developmental age or inflammation, and are expressed on many non-HSCs.[2-4] The recent identification of CD150/SLAM as stable markers made it possible to increase the purity of HSCs even in aged mice or cyclophosphamide/granulocyte colony-stimulating factor-treated mice with mobilized progenitors.[5] However, even the most highly purified HSCs are heterogeneous, and it may eventually be possible to associate discrete functions or activity states with subpopulations. Additional authentic HSC markers could have utility in attempts to rescue hematopoietic disorders using hematopoietic progenitors obtained from reprogrammed adult tissues.[6,7]

HSCs are thought to arise initially from hemogenic endothelium, which can produce hematopoietic cells as well as endothelial cells. Therefore, it is not surprising that HSCs share some endothelial properties at early developmental stages.[8,9] For example, the CD34 sialomucin and Tie2, an angiopoietin receptor, are expressed on HSCs in E10–11 embryos.[10,11] Endoglin and vascular-endothelial cadherin are additional endothelial markers found on fetal HSCs.[8,12] However, the expression of many of these antigens declines on HSCs at later stages of development.[3,4,13] It is interesting that the expression of CD34 is restored when adult HSCs are driven into cycle by 5-fluorouracil or granulocyte colony-stimulating factor administration.[14,15] CD11b/Mac-1 is an adhesion molecule that is similarly dependent on developmental age and activation status.[16] In contrast to these patterns, endomucin is a CD34-like sialomucin that marks HSCs from E10 and throughout subsequent development.[17] Each of these advances offered the promise of learning more about how HSCs arise de novo and function throughout life.

We previously determined that the most primitive cells with lymphopoietic potential first develop in the para-aortic splanchnopleura (PSp)/aorta-gonad-mesonephros (AGM) region of embryos, and we tracked expression of the *Rag1* lymphoid gene.[18,19] To extend those findings, we searched for genes that might be differentially expressed at the very earliest stages of lymphopoiesis. We here show that endothelial cell-selective adhesion molecule (ESAM) is a durable and effective marker of HSCs. Indeed, ESAM was expressed throughout life and could be used as a gating parameter for sorting long-term repopulating HSCs.

Methods

Animals

Rag1/GFP knockin mice (CD45.2 alloantigen) were described.[20,21] Mice of the corresponding wild-type (WT) C57BL/6 were obtained from Japan Clea (Shizuoka, Japan). Mating homozygous male Rag1/GFP knockin mice with WT C57BL/6 female mice generated heterozygous Rag1/GFP knockin

Submitted July 4, 2008; accepted November 1, 2008. Prepublished online as *Blood* First Edition paper, December 18, 2008; DOI 10.1182/blood-2008-07-167106.

An Inside *Blood* analysis of this article appears at the front of this issue.

The online version of this article contains a data supplement.

The publication costs of this article were defrayed in part by page charge payment. Therefore, and solely to indicate this fact, this article is hereby marked "advertisement" in accordance with 18 USC section 1734.

fetuses. The day of vaginal plug observation was considered as day 0.5 postcoitum (E0.5). In some experiments, we purchased pregnant C57BL/6 mice from Japan Clea and used their fetuses. The congenic C57BL/6 strain (C57BL/6SJL; CD45.1 alloantigen) was purchased from The Jackson Laboratory (Bar Harbor, ME) and used in transplantation experiments. The experimental designs of this study were approved by the committee of Osaka University for animal studies.

Antibodies

Phycoerythrin (PE)–conjugated anti-Sca1 (Ly6A/E; D7), CD48 (HM48-1), CD11b/Mac-1 (M1/70), Gr-1 (RB6-8C5), CD19 (1D3), CD4 (L3T4), and CD8a (53-6.7) monoclonal antibodies (mAbs), biotinylated anti-CD45.2(104) mAb, allophycocyanin (APC)–conjugated anti-CD11b/Mac-1 (M1/70) and c-kit (2B8) mAbs, and PE-Texas red tandem-conjugated (PE-TR) streptavidin were purchased from BD Biosciences PharMingen (San Diego, CA). PE-conjugated anti-CD34 (RAM34), CD31/PECAM-1(390), CD105/Endoglin (MJ7/18), and Tie2 (TEK4) mAbs, PE-Cy7–conjugated anti-Sca1 (Ly6A/E; D7) mAb, and APC-conjugated anti CD45.1 (A20) mAbs were purchased from eBioscience (San Diego, CA). A rat anti–mouse ESAM mAb (1G8), a rabbit anti–mouse ESAM polyclonal Ab (VE19), and a rabbit preimmune IgG were prepared in our hands.[22] A fluorescein isothiocyanate (FITC)–conjugated goat anti–rat IgG (H+L) Ab purchased from Southern Biotechnology (Birmingham, AL), a PE-conjugated goat antirat Ig Ab purchased from BD Biosciences PharMingen, or AlexaFluor 488 goat anti–rabbit IgG (H+L) Ab purchased from Invitrogen (Carlsbad, CA) was used as a second Ab for the anti-ESAM Abs. A PE-conjugated hamster IgG1 was purchased from BD Biosciences PharMingen and used as a control for a PE-conjugated anti-CD48. FITC-conjugated anti-CD11b/Mac-1 (M1/70), Gr-1 (RB6–8C5), TER-119, CD45R/B220 (RA3-6B2), and CD3e (145-2C11) were purchased from BD Biosciences PharMingen and used as lineage markers in adult studies.

Cell sorting

Fetal liver or cells obtained from adult femurs and tibias of heterozygous Rag1/GFP knockin mice were harvested and subjected to cell sorting as previously described.[18] In the first step, Rag1$^-$ or Rag1^{Lo} cells were sorted according to levels of green fluorescent protein (GFP) expression. Background auto-fluorescence was discriminated from authentic GFP by collecting data in 2 fluorescence channels without compensation. Under these conditions, even extremely low levels of fluorescence specific to GFP knockin mice were obvious on 2-color diagonal plots. The purity of the sorted cells in the first step was more than 95%. The sorted cells were incubated with anti-FcR (2.4G2) before staining with PE-anti-Sca1 and APC-anti-c-kit antibodies, suspended in 7-amino-actinomycin D (7-AAD)–containing buffer, and subjected to a second round of sorting. Dead cells stained with 7-AAD and a few contaminating cells with inappropriate GFP levels were gated out, and the cells were then fractionated according to Sca1 and c-kit to obtain Rag1$^-$ c-kit^{Hi} Sca1$^+$ HSCs and Rag1^{Lo} ckit^{Hi} Sca1$^+$, early lymphoid progenitors (ELPs). The cell sorting was performed with FACSaria using the FACSDiva program (BD Biosciences, San Jose, CA). The sorting gates used to isolate HSCs and ELPs from E14.5 fetal liver for gene array experiments ("Gene arrays") are shown in Figure S1 (available on the *Blood* website; see the Supplemental Materials link at the top of the online article).

In the sorting experiments with ESAM expression, Rag1/GFP$^-$ cells were first sorted from fetal tissues or adult bone marrow. Then the cells were stained with rat anti–mouse ESAM mAb (1G8) followed by FITC-goat anti–rat IgG or PE-goat anti–rat Ig, respectively. After the staining for ESAM, E14.5 fetal liver Rag1/GFP$^-$ cells were stained with PE–anti-Sca1 and APC-anti–c-kit antibodies. For PSp/AGM or yolk sac (YS) cells of E9.5-10.5 embryos, a PE-anti–Tie2 Ab was used instead of a PE-anti–Sca1 Ab. The adult marrow Rag1/GFP$^-$ cells were stained with FITC-anti-Lin (Mac-1, Gr-1, TER119, CD45R/B220, CD3e), PE-Cy7–anti-Sca1, and APC-anti–c-kit Abs. Then the cells were suspended in 7-AAD–containing buffer and subjected to a second round of sorting.

Gene arrays

Total RNAs were isolated from the Rag1$^-$ ckit^{Hi} Sca1$^+$, HSC-enriched fraction and the Rag1^{Lo} ckit^{Hi} Sca1$^+$, ELP-enriched fraction, both of which were isolated from mouse E14.5 fetal liver. From the aliquot of each RNA (24 ng), biotin-labeled cRNA was prepared using GeneChip 2-Cycle Target Labeling and Control Reagents (Affymetrix, Santa Clara, CA) according to the manual. The cRNA was fragmented and hybridized to Mouse Genome 430 2.0 Array (Affymetrix) using a GeneChip Hybridization, Wash, and Stain Kit (Affymetrix). Fluorescent signals were scanned by GeneChip Scanner 3000, and the data were analyzed by GeneSpring GX software (Agilent Technologies, Palo Alto, CA). *Bacillus subtilis* genes on the arrays were used as negative controls for background subtraction. All values of the genes in each array were divided by the value of glyceraldehyde-3-phosphate dehydrogenase (*Gapdh*) gene. The Cross-Gene Error Model was used to estimate measurement precision by combining variability of gene expression data. The experiments were duplicated to confirm reproducibility of the data. All microarray data have been deposited with CIBEX, National Institute of Genetics DDBJ (DNA Data Bank of Japan) under the accession number CBX73.

Flow cytometry

Rag1/GFP$^-$ cells of E14.5 fetal liver were incubated with rat anti–mouse ESAM mAb (1G8) followed by FITC-goat anti–rat IgG. Then the cells were incubated with a rat anti–mouse FcRII/III (2.4G2) and subsequently stained with PE-Cy7–anti-Sca1 and APC-anti–c-kit in combination with PE-anti–CD34, CD31/PECAM1, CD105/Endoglin, or Tie2 mAbs. The cells were suspended in 7-AAD–containing buffer and subjected to flow cytometry analyses, performed with FACSaria using the FACSDiva program (BD Biosciences).

In the other experiments, cultured cells or recovered cells from transplanted mice were incubated with anti-FcR and then stained with PE-, APC-conjugated mAbs and/or a biotinylated Ab followed by PE-TR-streptavidin as indicated in each figure. The flow cytometry analyses were performed with FACScalibur using the Cellquest program (BD Biosciences). The data analyses were done with FlowJo software (TreeStar, Ashland, OR).

Methylcellulose culture

A total of 500 or 100 cells of each sorted fraction (Rag1/GFP$^-$ ckit^{Hi} Sca1$^+$ ESAM1$^{-/Lo}$ or Rag1/GFP$^-$ ckit^{Hi} Sca1$^+$ ESAM1^{Hi} of fetal liver or adult marrow, respectively) were cultured in Iscove modified Dulbecco medium-based methylcellulose medium supplemented with 50 ng/mL of recombinant mouse (rm) stem cell factor (SCF), 10 ng/mL of rm interleukin-3 (IL-3), 10 ng/mL of recombinant human IL-6, and 3 U/mL of recombinant human erythropoietin (Methocult GF 3434; StemCell Technologies, Vancouver, BC). After 8 to 10 days, colonies were enumerated and classified as granulocyte colony-forming units (CFU-G); macrophage colony-forming units (CFU-M); granulocyte-macrophage colony-forming units (CFU-GM); erythroid burst-forming units (BFU-E); or mixed erythroid-myeloid colony-forming units (CFU-Mix) according to shape and color under an inverted microscope. In some experiments, colony types were morphologically certified by examination of cytospin preparations after May-Grünwald/Giemsa staining.

Stromal coculture and limiting dilution assays

The murine bone marrow stromal cell line MS-5 was generously provided by Dr J. Mori (Niigata University, Niigata, Japan). Nonirradiated MS-5 stromal cells were prepared at a concentration of 5×10^4 cells/well in 24-well tissue plates 1 day before the seeding of sorted cells at a concentration of 50 cells/mL. Cells were cultured in α-minimum essential medium (Invitrogen) supplemented with 10% fetal calf serum (FCS), rm SCF (10 ng/mL), rm Flt3-ligand (20 ng/mL), and rm IL-7 (1 ng/mL). The cultures were fed every 4 days by removing half of the medium and replacing it with fresh medium, and maintained for 6 or 10 days. Cytokines were freshly added with each feeding.

The frequencies of lymphohematopoietic progenitors in the fetal liver–derived Rag1/GFP$^-$ ckit^{Hi} Sca1$^+$ ESAM$^{-/Lo}$ or Rag1/GFP$^-$ ckit^{Hi} Sca1$^+$ ESAM^{Hi} fraction were determined by plating the sorted cells in limiting dilution assays using 96-well flat bottom plates. Pre-established MS-5 stromal cell layers were plated with 1, 2, 4, 8, or 50 cells each using the Automated Cell Deposition Unit of the FACSaria (BD Biosciences). Cells were cultured in α-minimum essential medium supplemented with 10% FCS, rm SCF (10 ng/mL), rm Flt3-ligand (20 ng/mL), and rm IL-7 (1 ng/mL). At 10 days of culture, wells were inspected for the presence of hematopoietic clones. Positive wells were harvested, stained, and analyzed by flow cytometry for the presence of CD19$^+$ Gr-1$^-$ B lineage cells. The frequencies of progenitors were calculated by linear regression analysis on the basis of Poisson distribution as the reciprocal of the concentration of test cells that gave 37% negative cultures.

Competitive repopulation assay

The Ly5 system was adapted to a competitive repopulation assay. A total of 1000 Rag1/GFP$^-$ c-kit^{Hi} Sca1$^+$ ESAM$^{-/Lo}$ or Rag1/GFP$^-$ c-kit^{Hi} Sca1$^+$ ESAM^{Hi} cells sorted from fetal liver of E14.5 Rag1/GFP heterozygous embryos (CD45.2) were mixed with 2×10^5 unfractionated adult bone marrow cells obtained from WT C57BL/6-Ly5.1 (CD45.1) mice and were transplanted into C57BL/6-Ly5.1 mice irradiated at a dose of 10 Gy. At 5 weeks after transplantation, peripheral blood cells of the recipients were colleted by retro-orbital bleeding and were stained with APC-conjugated anti-CD45.1 and biotinylated anti-CD45.2 Abs followed by PE-TR streptavidin. The cells were simultaneously stained with PE-conjugated anti–Mac-1 and Gr-1 Abs, or PE-conjugated anti-CD19 Ab, or PE-conjugated anti-CD4 and CD8a Abs. Twenty weeks after transplantation, all recipients were killed, and reconstitution of CD45.2$^+$ myeloid, B, or T cells was confirmed by flow cytometry in the bone marrow, spleen, and thymus, respectively. For the second transplantation, bone marrow cells of primary recipients with CD45.2 engraftment were transferred into 10 Gy-irradiated C57BL/6-Ly5.1 mice (10^6 whole bone marrow cells per recipient). After 20 weeks, contribution of CD45.2 cells to the hematopoietic reconstitution was evaluated in the second recipients.

Cell preparation from PSp/AGM and YS

To examine the phenotype or function of hematopoietic progenitors in the PSp/AGM and the YS of early embryos, cells were prepared as previously described.[19] Briefly, tissues were dissociated by incubation with dispase II (Roche Diagnostics, Mannheim, Germany) for 20 minutes at 37°C and cell dissociation buffer (Invitrogen) for 20 minutes at 37°C followed by vigorous pipetting. The cells were then suspended in phosphate-buffered saline containing 3% FCS and stained with the Abs indicated in each experiment.

Statistical methods

Statistical analysis was carried out by standard Student *t* tests. Error bars used throughout indicate SD of the mean.

Results

Identification of ESAM as a marker of primitive hematopoietic cells

Microarrays were performed as part of an effort to characterize the initial transition of fetal HSCs to primitive lymphopoietic cells. The comparisons involved mRNA from Rag1^{Lo} ckit^{Hi} Sca1$^+$, ELPs, and the HSC-enriched Rag1$^-$ ckit^{Hi} Sca1$^+$ fraction isolated from E14.5 fetal liver (Figure S1).

Consistent with previous analyses,[12,23,24] *Evi1*, *CD41*, and *Endoglin* were highly expressed by fetal HSCs (Figure 1). *Esam* transcripts were conspicuous in the HSC fraction and attracted attention because of a sharp down-regulation on differentiation to ELP (Figure 1). Real-time PCR using *Esam* specific primers verified the results of these microarrays (data not shown).

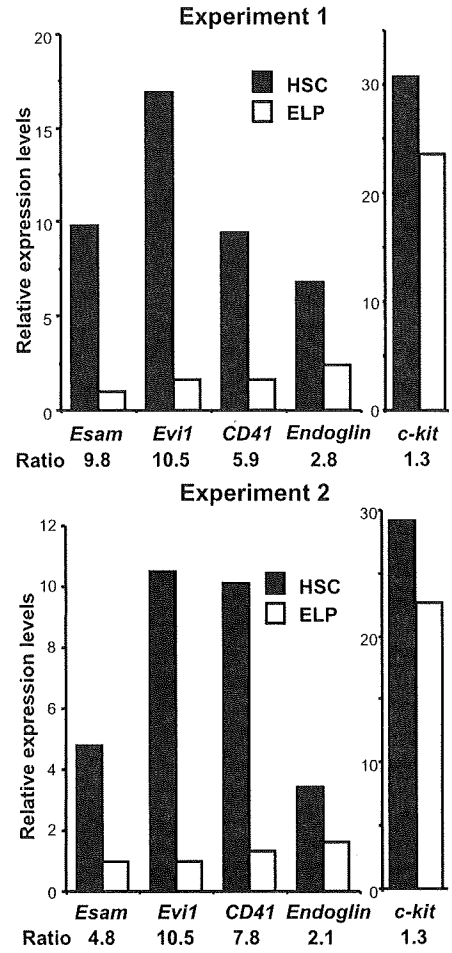

Figure 1. *Esam* gene is preferentially expressed in the HSC fraction of E14.5 fetal liver. Microarray analyses comparing HSC-enriched and ELP-enriched populations were performed. Two independent tests depicted the *Esam* gene as preferentially expressed in the HSC-enriched population. Results are shown as relative expression levels of each gene comparing with that of *Gapdh* of which value is 100. Ratio was calculated by [HSC level]/[ELP level] in each gene. The relative expression levels of *c-kit* were also shown as internal quality controls.

ESAM can be used to subdivide hematopoietic progenitors in fetal liver

The availability of a rat antimouse ESAM mAb (clone 1G8) facilitated characterization of mononuclear cells obtained from E14.5 fetal liver. A majority of ESAM$^+$ cells were found in the c-kit^{Hi} fraction (Figure 2A left). ESAM expression also correlated with Sca1 (Figure 2A middle). These observations suggested that ESAM might substitute for at least one of the 2 most widely used HSC markers. Indeed, cells in the Sca1^{Hi} ESAM^{Hi} gate were almost homogeneous with respect to high c-kit expression (Figure 2A right).

The c-kit^{Hi} Sca1$^+$ fraction, known to include all conventional HSCs, was divided into 2 categories according to ESAM staining (Figure 2B left and middle). The subpopulation with the highest density of ESAM was enriched for c-kit^{Hi} Sca1^{Hi} cells, whereas ones with negative or low levels of ESAM were found in the c-kit^{Hi} Sca1^{Lo} subset (Figure 2B right). The latter are thought to be enriched with respect to committed myelo-erythroid progenitors.[25] Similar results were obtained with a rabbit antimouse ESAM polyclonal Ab (VE19) (data not shown).

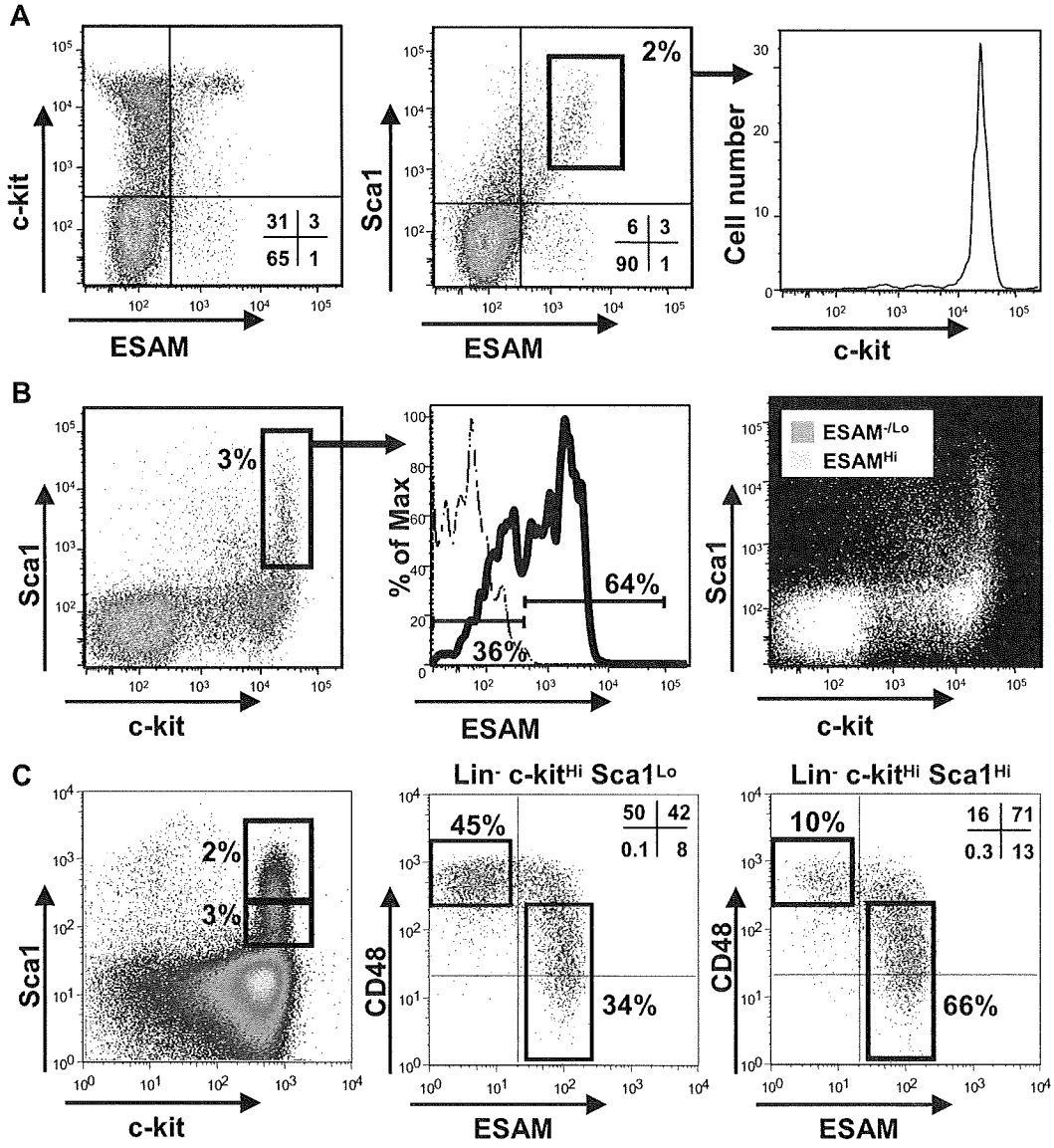

Figure 2. Specific expression of ESAM on HSC-enriched fraction of E14.5 fetal liver. Flow cytometric analysis was performed for Rag1/GFP$^-$ cells of E14.5 fetal liver using anti-c-kit, anti-Sca1, and anti-ESAM Abs. First, Rag1/GFP$^-$ cells were sorted from E14.5 fetal liver of Rag1/GFP knockin heterozygous fetuses with high purity. The sorted cells were incubated with a purified rat anti–mouse ESAM Ab (1G8) followed by goat anti–rat IgG-FITC. The cells were then stained with anti-c-kit-APC, anti-Sca1-PE, and 7-AAD. To minimize the nonspecific binding of anti-c-kit and Sca1 mAbs to the cells wearing goat anti–rat IgG-FITC, the cells were incubated with a rat anti–mouse FcRII/III Ab before the anti-c-kit and Sca1 staining. (A) The Rag1/GFP$^-$ cells were analyzed with respect to expression of ESAM, c-kit, and Sca1 (Left, middle). Expression of c-kit in the Sca1^{Hi} ESAM^{Hi} cells (middle, inset) is presented (right). (B) The conventional c-kit^{Hi} Sca1$^+$ fraction (left, inset) could be divided into 2 fractions, ESAM$^{-/Lo}$ and ESAM^{Hi} (middle). The cells were stained with an isotype control IgG (dashed line) or with the anti-ESAM Ab (solid line). The ESAM^{Hi} cells (yellow) were found as c-kit^{Hi} Sca1^{Hi}, whereas the ESAM$^{-/Lo}$ cells (pink) were c-kit^{Hi} Sca1^{Lo} (right). (C) Six-color flow cytometric analysis using an anti-ESAM Ab followed by goat anti–rat IgG-FITC, a PE-anti-CD48 Ab, biotin-anti-lineage marker Abs (TER119, Gr1, CD3, CD45R/B220) followed by SA-PETR, a PE-Cy7-anti-Sca1 Ab, an APC-anti-c-kit, and 7-AAD was performed for E14.5 fetal liver cells of WT C57B6 embryos. The profile of Lin$^-$ cells regarding c-kit and Sca1 expression is shown in the left. The Lin$^-$ c-kit^{Hi} Sca1^{Lo} and Lin$^-$ c-kit^{Hi} Sca1^{Hi} fractions gated in the left panel were analyzed with respect to expression of ESAM and CD48 (middle and right). The percentage of cells in each gate is indicated in each panel.

When E14.5 fetal liver cells of WT C57B6 mice and traditional markers of fetal liver HSCs were used instead of the Rag1/GFP knockin mice, essentially identical results were obtained (Figure 2C). This analysis was performed with CD48 expression, one of the SLAM family members recently shown to conversely relate with HSC activity in fetal liver.[26] Lin$^-$ c-kit^{Hi} Sca1$^+$ cells could be divided into ESAM$^-$ and ESAM$^+$ fractions, and a subpopulation with higher Sca1 expression was more enriched with ESAM$^+$ cells (Figure 2C middle and right). CD48 expression tended to increase along with down-regulation of ESAM. Indeed, the Lin$^-$ c-kit^{Hi} Sca1$^+$ fraction was found to consist of 2 major subpopulations, CD48^{Hi} ESAM$^-$ and CD48$^{-/Lo}$ ESAM$^+$. Thus, ESAM is conspicuously expressed on immature hematopoietic cells in fetal liver and seems to conversely relate to lineage progression.

ESAM expression is closely associated with fetal HSCs among endothelial markers

Next we evaluated how ESAM corresponds to other endothelial antigens that were previously identified on fetal hematopoietic progenitors. CD34 and CD31/PECAM1 were uniformly present on Rag1$^-$ c-kit^{Hi} Sca1$^+$ cells in E14.5 fetal liver (Figure 3A,B). Neither could resolve the Rag1$^-$ c-kit^{Hi} Sca1$^+$ cells into ESAM^{Hi} and ESAM$^{-/Lo}$ fractions, and even showed a slightly inverse relationship with ESAM expression on early progenitors. Expression profiles of Endoglin and

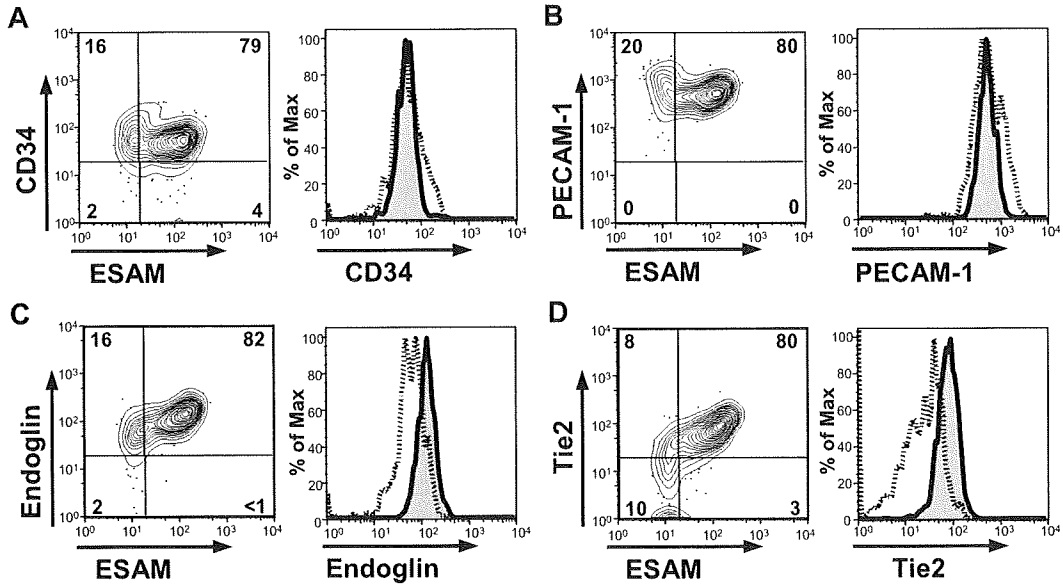

Figure 3. Expression of ESAM and other endothelial antigens on fetal liver HSC fraction. The expression pattern of ESAM on Rag1/GFP$^-$ c-kit^{Hi} Sca1$^+$ cells of E14.5 fetal liver was compared with other endothelial cell-related antigens, CD34 (A), CD31/PECAM1 (B), Endoglin (C), and Tie2 (D). The percentage of cells in subpopulation is shown. In the histograms, the staining patterns of ESAM$^{-/Lo}$ cells are indicated with dashed lines; those of ESAM^{Hi} cells are tinted and indicated with solid lines.

Tie2 did correlate with ESAM (Figure 3C,D). However, although the primitive ESAM^{Hi} fraction uniformly expressed high levels of Endoglin and Tie2, many of the more differentiated ESAM$^{-/Lo}$ cells still retained the 2 markers. These results suggest that ESAM might be a more useful marker of HSCs than other endothelial antigens and could represent an important tool for fetal stem cell studies.

ESAM is useful to enrich primitive multipotent progenitors from fetal liver

To evaluate whether ESAM expression can enrich primitive progenitors in fetuses, we compared the clonogenic potential in methylcellulose cultures of the ESAM$^{-/Lo}$ and ESAM^{Hi} cells in the Rag1$^-$ ckit^{Hi} Sca1$^+$ HSC fraction of E14.5 fetal liver. Cells in the ESAM^{Hi} fraction formed more colonies with larger size than those in the ESAM$^{-/Lo}$ fraction (Figure 4). In particular, most CFU-Mix, primitive progenitors with both myeloid and erythroid potential, were found in the ESAM^{Hi} fraction (Figure 4A).

Next we analyzed the lymphopoietic potential of cells resolved on the basis of ESAM in cocultures with the MS5 bone marrow stromal cell line. The culture media contained SCF, Flt3-ligand, and IL-7, factors that effectively generate CD19$^+$ B lymphoid cells as well as Mac1$^+$ myeloid cells.[18] When 500 cells were cultured in individual wells of 6-well plates, both ESAM$^{-/Lo}$ and ESAM^{Hi} fractions produced CD19$^+$ cells and Mac1$^+$ cells (Figure 5A). However, we observed that most of the hematopoietic colonies from ESAM^{Hi} cells grew beneath the MS5 stromal cell layer, although this was not the case with ESAM$^{-/Lo}$ cells (data not shown). Moreover, the lymphohematopoietic cells from ESAM^{Hi} cells continued to expand explosively after 6 days of coculture and gave rise to approximately 50 000 cells per input progenitor by day 10 (Figure 5B).

Authentic HSCs are characterized as having both lymphoid and myeloid potential.[8,27] To compare numbers of primitive lymphohematopoietic progenitors in the ESAM^{Hi} and ESAM$^{-/Lo}$ fractions, we performed in vitro limiting dilution assays in MS5 cocultures. One in 2.1 ESAM^{Hi} cells and 1 in 3.5 ESAM$^{-/Lo}$ cells gave rise to blood cells, indicating that both fractions are extremely potent sources of hematopoietic progenitors (Figure 5C left). However, we observed drastic differences between the 2 fractions regarding the frequencies of primitive progenitors with lymphopoietic potential. Whereas 1 in 8 ESAM^{Hi} cells produced CD19$^+$ B lineage cells, only 1 in 125 ESAM$^{-/Lo}$ cells were lymphopoietic under these conditions (Figure 5C right). These results suggest that primitive

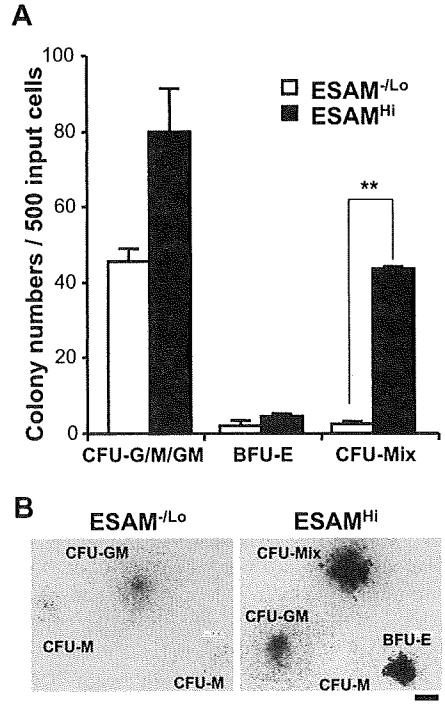

Figure 4. ESAM expression correlates with CFU activity. ESAM$^{-/Lo}$ or ESAM^{Hi} cells of the Rag1/GFP$^-$ ckit^{Hi} Sca1$^+$ fraction of E14.5 fetal liver were sorted and subjected to methylcellulose colony formation assay. Numbers of CFUs (A) and morphology of the colonies derived from the indicated CFUs (B) are shown. The results in panel A are shown as mean plus or minus SD. A black bar in panel B represents 500 mm. The data are from one of 3 independent experiments that gave similar results. Significant difference between the 2 population is indicated (**$P < .01$).

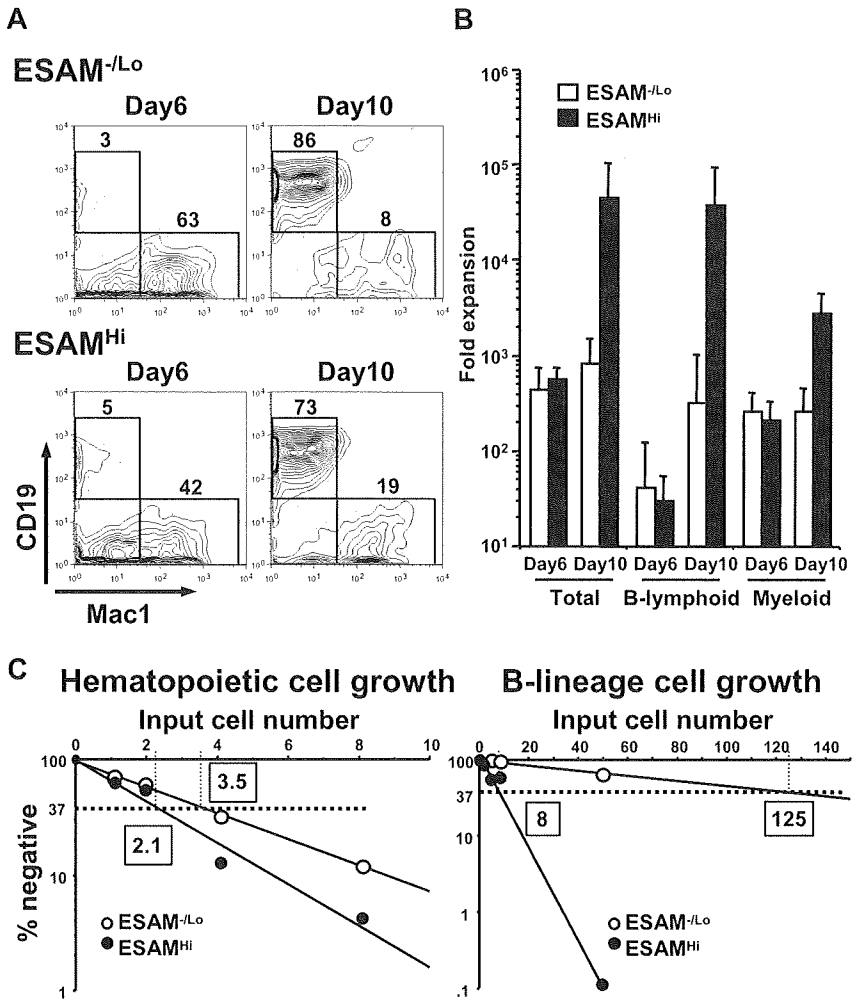

Figure 5. ESAM expression enriches primitive progenitors endowed with lymphopoietic activity. (A,B) A total of 500 ESAM$^{-/Lo}$ or ESAM^{Hi} cells of the Rag1/GFP^{-} ckit^{Hi} Sca1^{+} fraction of E14.5 fetal liver were cultured with MS5 stromal cells in the presence of SCF, Flt3-ligand, and IL-7. At the indicated period, recovered cells were counted and subjected to flow cytometry (A). Yields of total cells, CD19^{+} Mac1^{-} B-lineage cells, and Mac1^{+} CD19^{-} myeloid-lineage cells per 1 input ESAM$^{-/Lo}$ or ESAM^{Hi} progenitor were calculated and given as averages with SD bars (B). (C) Limiting dilution analyses were performed in the MS5 coculture system to determine the frequency of hematopoietic progenitors (left) and that of progenitors endowed with lymphopoietic potential (right).

stem/progenitor cells, which are multipotent for myeloid, erythroid, and lymphoid lineages, are present in the ESAM^{Hi} fraction of fetal liver.

Long-term reconstitution activity is exclusive to ESAM^{Hi} cells

To evaluate ESAM expression on long-term reconstituting HSCs in E14.5 fetal liver, we transplanted cells of the ESAM$^{-/Lo}$ or ESAM^{Hi} fraction into lethally irradiated mice (Figure 6A). Five weeks after transplantation, it was obvious that CD45.2^{+} ESAM^{Hi} cells contributed highly to the recovery of hematopoiesis in recipients, but no chimerism was detected in mice transplanted with ESAM$^{-/Lo}$ cells (Figure 6B). Indeed, although 9 of 11 mice transplanted with 1000 ESAM^{Hi} cells had clear donor CD45.2^{+} populations ($> 1.0\%$) among peripheral leukocytes, none of 10 mice given 1000 ESAM$^{-/Lo}$ cells had evidence of chimerism. Five months after transplantation, we analyzed the contribution of CD45.2^{+} cells to long-term lymphohematopoietic reconstitution of the recipients. Although most of the 11 mice transplanted with ESAM^{Hi} cells had clear CD45.2^{+} populations in bone marrow (mean $\pm$ SD of percentage CD45.2^{+} CD45.1^{-} in total CD45^{+} cells; 16.3% $\pm$ 22.0%), none of the ESAM$^{-/Lo}$-transplanted mice contained detectable CD45.2^{+} cells in that organ (mean $\pm$ SD of percentage CD45.2^{+} CD45.1^{-} in total CD45^{+} cells; 0.02% $\pm$ 0.03%) (Figure 6C). Furthermore, multilineage recovery was observed in the bone marrow, spleen, and thymus of mice transplanted with ESAM^{Hi} cells (Figure 6D). In addition, bone marrow cells recovered from primary recipients with ESAM^{Hi} cell transplantation effectively reconstituted CD45.2^{+} lymphohematopoietic cells in secondary recipients at 5 months after transplantation (data not shown). These results indicate that high levels of ESAM expression correspond to fetal HSCs with long-term repopulating potential.

ESAM expression marks cells thought to represent HSCs in fetal and aged adult tissues

The definitive HSCs that account for lymphohematopoieisis in adults first arise in the AGM region.[28,29] To examine whether ESAM was present on those HSCs, flow cytometry analyses were performed with the Rag1/GFP^{-} cells isolated from E10.5 embryos. Tie2 and c-kit were used as additional parameters because we previously identified lymphohematopoietic cells in the early embryos as Rag1^{-} Tie2^{+} c-kit^{+}.[19] A small but conspicuous Tie2^{Hi} population was detected in E10.5 AGM cells (Figure 7A left). Interestingly, the Tie2^{Hi} AGM cells were clearly divided into 2 discrete populations according to ESAM expression (Figure 7A middle). When the 2 populations were back-plotted on the Tie2 and c-kit profile, ESAM^{+} cells were exclusively c-kit^{+} (Figure 7A right). In addition, lymphohematopoietic potential in the MS5 cocultures was highly enriched in the ESAM^{+} fraction among the Tie2^{Hi} cells. That is, the Tie2^{Hi} ESAM^{+} fraction could effectively produce both CD19^{+} lymphoid cells and Mac1^{+} myeloid cells, although the Tie2^{Hi} ESAM^{-} fraction generated only a small

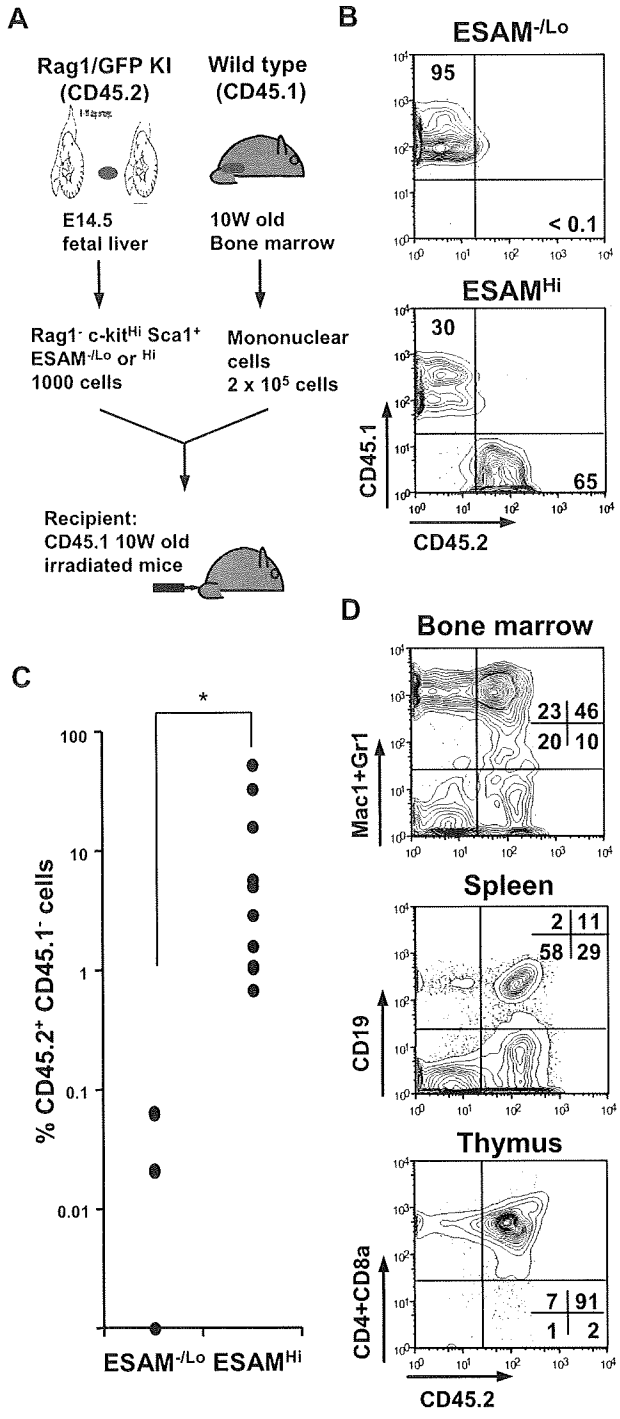

Figure 6. Long-term hematopoiesis-reconstituting activity is excusive to ESAM^{Hi} fraction. (A) The Rag1/GFP$^-$ Sca1$^+$ c-kit^{Hi} cells (CD45.2$^+$) of E14.5 fetal liver were sorted into 2 fractions, ESAM$^{-/Lo}$ and ESAM^{Hi}. Then, 1000 cells of each fraction were mixed with 2×10^5 CD45.1$^+$ whole adult bone marrow cells of 10-week-old mice and transplanted to a lethally irradiated CD45.1 mouse (A). (B) Flow cytometry analyses for peripheral leukocytes were performed at 5 weeks after transplantation. In the 2 independent experiments, 9 of 11 recipients with ESAM^{Hi} cells were clearly reconstituted by CD45.2$^+$ cells (> 1.0% in all of myeloid, T, and B lineages), whereas none of 11 recipients with ESAM$^{-/Lo}$ cells had CD45.2$^+$ cells detectable in the flow cytometry. The figure shows representative results in each group. (C,D) Twenty weeks after transplantation, all the recipients were killed, and the contribution of CD45.2$^+$ ESAM^{Hi} cells was evaluated in lymphohematopoietic organs. Percentages of CD45.2$^+$ CD45.1$^-$ population among total CD45$^+$ cells in bone marrow of each recipient were plotted (C). The long-term reconstitution of CD45.2$^+$ ESAM^{Hi} cells was confirmed with respect to myeloid, B lymphoid, or T lymphoid lineages in the bone marrow, spleen, and thymus, respectively (D).

number of Mac1$^+$ cells (Figure 7B). We concluded from these analyses that ESAM marks the primitive hematopoietic cells endowed with lymphopoietic activity in the E10.5 AGM as well as in the E14.5 liver.

A small number of Tie2^{Hi} c-kit^{Lo} ESAM^{Hi} cells were also observed among extraembryonic YS cells (Figure 7C). In addition, the E10.5 YS contained a conspicuous population whose phenotype was Tie2^{Lo} c-kit^{Hi}, and cells in that fraction expressed low levels of ESAM (Figure 7C). Cells with the same phenotype were also clearly observed in the E9.5 YS, although they were absent in the caudal half of the embryo proper (Figure S2A). These Tie2^{Lo} c-kit^{Hi} ESAM^{Lo} cells in the YS effectively produced myeloid and/or erythroid colonies in methylcellulose culture but showed little lymphopoietic potential (Figure S2B,C). Importantly, lymphopoietic activity was exclusive to the Tie2^{Hi} c-kit^{Lo} ESAM^{Hi} fraction of the PSp/AGM region, which showed no myeloid-erythroid potential in conventional methylcellulose assays.

It is well known that HSC properties change with developmental age. Indeed, Forsberg et al previously reported ESAM expression by adult marrow HSCs,[30] but the levels were weak compared with those on fetal HSCs. Therefore, we expected that ESAM, like the other endothelial antigens, would decline with HSC aging. However, we found that ESAM expression was detectable on the Rag1$^-$ LSK fraction of bone marrow through life (Figure 7D). Indeed, the proportion of ESAM^{Hi} cells and the mean fluorescence intensity of ESAM expression in the Rag1$^-$ LSK fraction increased with age (Figure 7D). Moreover, primitive myeloid-erythroid progenitors from adult bone marrow were also enriched in the ESAM^{Hi} fraction (Figure 7E). In summary, these findings demonstrate that ESAM expression is useful for exploring the biology of hematopoietic stem/progenitor cells throughout life in mice.

Discussion

We conducted gene array analyses with the principal goal of learning more about the initial differentiation of fetal HSCs to cells in lymphoid lineages. In that regard, several informative genes were identified and will be presented elsewhere (manuscript in preparation). Our screen also identified genes whose expression was previously thought to correlate with HSCs in fetal or adult tissues. Among those, *Esam* was particularly noteworthy as being drastically down-regulated during differentiation of HSCs to ELPs. We now report that it represents a potent tool for identifying HSCs over a wide range of developmental age.

ESAM was originally identified as an endothelial cell-specific protein, although it was also shown to be expressed on megakaryocytes and platelets.[22,31] A recent study also found ESAM transcripts in adult marrow HSCs when gene arrays were used to compare Thy1.1^{Lo} Flk2$^-$ LSK (long-term HSC-enriched), Thy1.1^{Lo} Flk2$^+$ LSK (short-term HSCs), and Thy1.1$^-$ Flk2$^+$ LSK (multiple progenitors).[30] We now show how ESAM levels can be exploited to obtain highly enriched CFU-Mix, lymphopoietic cells, and long-term HSCs from the Rag1$^-$ c-kit^{Hi} Sca1$^+$ fraction of E14.5 fetal liver. It is important to note that long-term HSCs in mouse embryos are unique in expressing markers, such as Flk2 and CD11b/Mac1, not characteristic of adult HSCs.[18,32] This complicates cell sorting strategies and fetal/adult comparison. We previously found that Rag1/GFP$^-$ c-kit^{Hi} Sca1$^+$ cells derived from E14.5 fetal liver reconstituted lymphohematopoiesis in lethally irradiated adults, whereas Rag1/GFP^{Lo} c-kit^{Hi} Sca1$^+$ cells transiently contributed to T and B lymphopoiesis. ESAM specific Abs can be used without

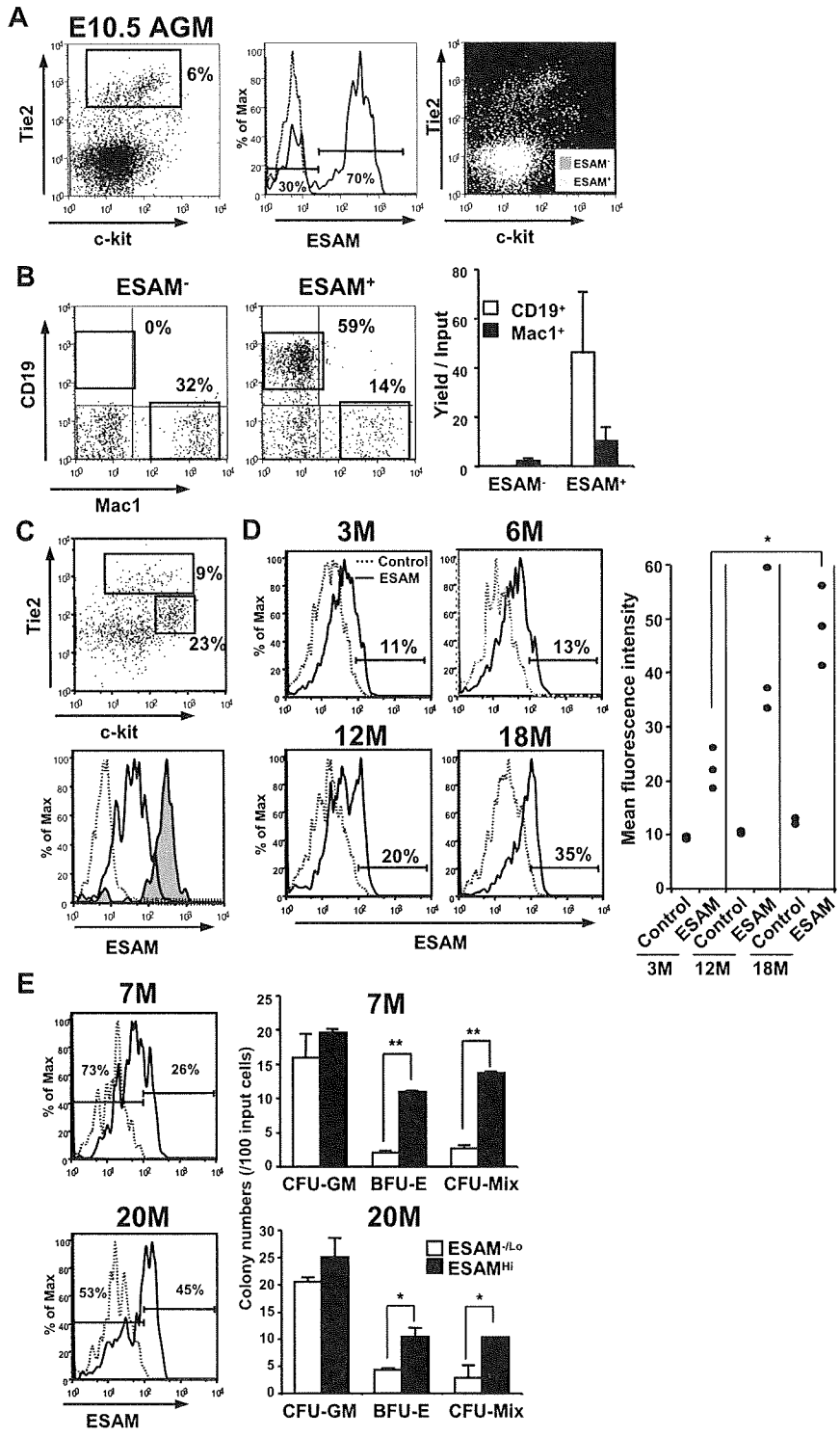

Figure 7. ESAM marks early hematopoietic progenitors throughout life. (A) Rag1/GFP$^-$ cells were sorted from AGM of E10.5 Rag1/GFP knockin heterozygous fetuses with high purity. The sorted Rag1/GFP$^-$ cells were incubated with the anti-ESAM Ab (1G8) followed by goat antirat IgG-FITC. The cells were then stained with anti-c-kit-APC, anti-Tie2-PE, and 7-AAD. The profile of Tie2 and c-kit expression in AGM cells was shown in a left panel. ESAM expression (solid line) in the Tie2^{Hi} fraction of AGM and its control level with an isotype-matched IgG (dashed line) are presented (middle). The Tie2^{Hi} ESAM$^+$ cells (yellow) were c-kit$^+$, whereas the Tie2^{Hi} ESAM$^-$ cells (pink) were c-kit$^-$ (right). (B) The Tie2^{Hi} ESAM$^-$ and Tie2^{Hi} ESAM$^+$ cells were sorted from E10.5 AGM and cultured on MS5 for 10 days. The recovered cells were counted and stained for the markers, including CD19 and Mac1. (C) Rag1/GFP$^-$ cells sorted from E10.5 YS were stained in the same manner as for the E10.5 AGM cells described in panel A. The profile of Tie2 and c-kit expression is shown in the top panel. In the lower panel, ESAM expression in the Tie2^{Hi} c-kit^{Lo} fraction (tinted histogram) and the Tie2^{Lo} c-kit^{Hi} fraction (open histogram) is shown. A dashed line shows the background fluorescence with an isotype-matched IgG. (D) ESAM expression of Rag1/GFP$^-$ Lin$^-$ ckit^{Hi} Sca1$^+$ cells of adult bone marrow of 3-, 6-, 12-, and 18-month-old mice was analyzed. Representative flow cytometry results in 3 to 5 mice of each age were shown. ESAM expression on Rag1/GFP$^-$ Lin$^-$ c-kit^{Hi} Sca1$^+$ cells of adult bone marrow of 3-, 12-, and 18-month-old mice (n = 3 in each) were simultaneously analyzed, and the data were summarized with respect to the mean fluorescence intensity with an anti-ESAM Ab or its control Ab (right panel). (E) ESAM$^{-/Lo}$ or ESAM^{Hi} cells were sorted from the Rag1/GFP$^-$ Lin$^-$ ckit^{Hi} Sca1$^+$ fraction of the indicated adult bone marrow (7 and 20 months old, respectively) and subjected to methylcellulose colony assay. The data are from one of 2 independent experiments that gave similar results. Statistical significance: $^*P < .05$, $^{**}P < .01$. The percentages of cells in each gate are indicated in each panel.

knockin reporters and with fewer combinations of Abs to obtain highly enriched HSCs.

Although we identified *Esam* as one of the highly expressed genes in HSC but not in ELP, levels of this antigen strongly correlated with lymphopoietic activity. The ESAM^{Hi} fraction in Rag1$^-$ c-kit^{Hi} Sca1$^+$ cells of E14.5 fetal liver produced CD19$^+$ B-lineage cells more effectively and contained lymphopoietic progenitors with even higher frequency than the ESAM$^{-/Lo}$ fraction. The cells also gave rise to long-term reconstitution in both T and B lymphoid lineages in lethally irradiated recipients. Furthermore, in the PSp/AGM region, B lymphopoietic activity in culture was exclusive to the ESAM^{Hi} Tie2$^+$ fraction. From these observations, we conclude that ESAM expression indicates high lymphopoietic potential in HSCs of the fetal liver and hematopoietic cells arising in the AGM region. On the other hand, we presume from the sharp down-regulation in ELPs that ESAM is not necessary for early lymphoid differentiation.

We previously reported that the first lymphopoietic cells arise in a Tie2$^+$ c-kit$^+$ CD34$^{-/Lo}$ CD41$^-$ subset in the E8.5 PSp region.[19] In this report, we showed clear ESAM expression on lymphopoietic

cells contained in a Tie2^{Hi} c-kit^{+} subset of the E9.5 to E10.5 PSp/AGM. Lymphopoietic activity in early embryos is thought to associate closely with HSC development. Because the first HSCs have few reliable surface markers, high ESAM expression must be useful to monitor how the first HSCs are developing and moving to other sites. As an additional finding, we detected high myeloid-erythroid but little lymphopoietic potential in a Tie2^{Lo} ckit^{Hi} subset of the YS, whose expression level of ESAM was apparently low. We presume that ESAM^{Hi} Tie2^{Hi} c-kit^{+} cells in the PSp/AGM and ESAM^{Lo} Tie2^{Lo} c-kit^{Hi} cells in the YS differ in their origins and/or as development progresses. If combined with those cell surface markers, a newly described method to trace runt-related transcription factor 1-expressing cells would address several important issues related to "primitive" and "definitive" hematopoiesis.[33]

It is interesting to speculate that ESAM might be important for HSC functions. A previous study showed that ESAM mediates homophilic interactions between endothelial cells,[22] and endothelial cells must represent an important component of HSC-supportive niches in bone marrow.[34] A subsequent study of ESAM-deficient mice showed impaired migration of neutrophils through vascular walls after normal adhesion.[35] In addition, platelets from ESAM-deficient mice were less prone to disaggregation.[36] Thus, ESAM expressed by endothelial and/or stem cells could have functions associated with HSC adhesion and/or migration.

Osteoblastic stromal cells that line trabecular bone are thought to construct niches containing molecules needed to regulate HSC quiescence, proliferation, and differentiation in adult bone marrow.[37,38] Other findings indicate that HSCs also interact with sinusoidal endothelial cells at some distance from bones.[39,40] Osteoblastic and vascular niches probably function in complementary ways.[41,42] The fetal liver has no osteoblasts, and HSC niches have not been identified in that site. High level ESAM display suggests that it should be further explored within the context of endothelial-HSC interactions.

It was an unexpected but intriguing finding that ESAM levels correlate with the stem cell rich fraction even in 22-month-old mice. Although many endothelial antigens on HSCs decline with aging, endomucin and endothelial protein C receptor (CD201) have been reported to be adult HSC markers.[17,43] In humans, angiotensin-converting enzyme (CD143) was recently found to mark HSCs through embryonic and adult life.[44] However, ESAM seems unique in actually increasing with aging. Many genes involved in NO-mediated signal transduction, stress responses, and inflammation have been linked to HSC aging.[4] P-selectin is one of the most highly up-regulated of those stress-related genes. Of particular interest, P-selectin mediates some leukocyte-vascular endothelium interactions and leukocyte extravasation, functions also attributed to ESAM on neutrophils.[35] Recent reports showed that stem/progenitor cells continuously circulate outside bone marrow and can actively participate in innate immune responses.[45,46] Furthermore, platelets can use P-selectin to recruit marrow hematopoietic cells into sites of injury.[47] Although direct evidence is lacking at this moment, further study might implicate elevated ESAM levels in extramedullary migration of HSCs.

Efficient HSC-based therapies and the emerging field of regenerative medicine will benefit from learning more about what defines stem cells. Although patterns of expression of transcription factors and other intracellular proteins are informative, surface markers such as ESAM that are unique to HSCs have special utility.

Acknowledgment

The authors thank Drs N. Sakaguchi (Kumamoto University) and H. Igarashi (Kawasaki Medical School) for the Rag1/GFP knockin mice.

Authorship

Contribution: T.Y. conducted experiments and analyzed results; T.Y., K.O., P.W.K., and Y.K. designed the research plan and wrote the paper; S.B. and D.V. prepared anti-ESAM antibodies; K.K. and T.M. performed and analyzed microarrays.

Conflict-of-interest disclosure: The authors declare no competing financial interests.

Correspondence: Takafumi Yokota, Department of Hematology and Oncology, Osaka University Graduate School of Medicine, C9, 2-2 Yamadaoka, Suita, Osaka 565-0871, Japan; e-mail: yokotat@bldon.med.osaka-u.ac.jp.

References

1. Osawa M, Hanada K, Hamada H, Nakauchi H. Long-term lymphohematopoietic reconstitution by a single CD34-low/negative hematopoietic stem cell. Science. 1996;273:242-245.
2. Spangrude GJ, Brooks DM. Mouse strain variability in the expression of the hematopoietic stem cell antigen Ly-6A/E by bone marrow cells. Blood. 1993;82:3327-3332.
3. Ogawa M. Changing phenotypes of hematopoietic stem cells. Exp Hematol. 2002;30:3-6.
4. Chambers SM, Shaw CA, Gatza C, Fisk CJ, Donehower LA, Goodell MA. Aging hematopoietic stem cells decline in function and exhibit epigenetic dysregulation. PLoS Biol. 2007;5:e201.
5. Yilmaz OH, Kiel MJ, Morrison SJ. SLAM family markers are conserved among hematopoietic stem cells from old and reconstituted mice and markedly increase their purity. Blood. 2006;107:924-930.
6. Takahashi K, Tanabe K, Ohnuki M, et al. Induction of pluripotent stem cells from adult human fibroblasts by defined factors. Cell. 2007;131:861-872.
7. Hanna J, Wernig M, Markoulaki S, et al. Treatment of sickle cell anemia mouse model with iPS cells generated from autologous skin. Science. 2007;318:1920-1923.
8. Nishikawa SI, Nishikawa S, Kawamoto H, et al. In vitro generation of lymphohematopoietic cells from endothelial cells purified from murine embryos. Immunity. 1998;8:761-769.
9. Oberlin E, Tavian M, Blazsek I, Péault B. Blood-forming potential of vascular endothelium in the human embryo. Development. 2002;129:4147-4157.
10. Yoder MC, Hiatt K, Dutt P, Mukherjee P, Bodine DM, Orlic D. Characterization of definitive lymphohematopoietic stem cells in the day 9 murine yolk sac. Immunity. 1997;7:335-344.
11. Takakura N, Huang XL, Naruse T, et al. Critical role of the TIE2 endothelial cell receptor in the development of definitive hematopoiesis. Immunity. 1998;9:677-686.
12. Cho SK, Bourdeau A, Letarte M, Zúñiga-Pflücker JC. Expression and function of CD105 during the onset of hematopoiesis from Flk1(+) precursors. Blood. 2001;98:3635-3642.
13. Matsuoka S, Ebihara Y, Xu M, et al. CD34 expression on long-term repopulating hematopoietic stem cells changes during developmental stages. Blood. 2001;97:419-425.
14. Sato T, Laver JH, Ogawa M. Reversible expression of CD34 by murine hematopoietic stem cells. Blood. 1999;94:2548-2554.
15. Tajima F, Sato T, Laver JH, Ogawa M. CD34 expression by murine hematopoietic stem cells mobilized by granulocyte colony-stimulating factor. Blood. 2000;96:1989-1993.
16. Randall TD, Weissman IL. Phenotypic and functional changes induced at the clonal level in hematopoietic stem cells after 5-fluorouracil treatment. Blood. 1997;89:3596-3606.
17. Matsubara A, Iwama A, Yamazaki S, et al. Endomucin, a CD34-like sialomucin, marks hematopoietic stem cells throughout development. J Exp Med. 2005;202:1483-1492.
18. Yokota T, Kouro T, Hirose J, et al. Unique properties of fetal lymphoid progenitors identified according to RAG1 gene expression. Immunity. 2003;19:365-375.
19. Yokota T, Huang J, Tavian M, et al. Tracing the first waves of lymphopoiesis in mice. Development. 2006;133:2041-2051.

20. Kuwata N, Igarashi H, Ohmura T, Aizawa S, Sakaguchi N. Cutting edge: absence of expression of RAG1 in peritoneal B-1 cells detected by knocking into RAG1 locus with green fluorescent protein gene. J Immunol. 2001;163:6355-6359.
21. Igarashi H, Gregory SC, Yokota T, Sakaguchi N, Kincade PW. Transcription from the RAG1 locus marks the earliest lymphocyte progenitors in bone marrow. Immunity. 2002;17:117-130.
22. Nasdala I, Wolburg-Buchholz K, Wolburg H, et al. A transmembrane tight junction protein selectively expressed on endothelial cells and platelets. J Biol Chem. 2002;277:16294-16303.
23. Yuasa H, Oike Y, Iwama A, et al. Oncogenic transcription factor Evi1 regulates hematopoietic stem cell proliferation through GATA-2 expression. EMBO J. 2005;24:1976-1987.
24. Mikkola HK, Fujiwara Y, Schlaeger TM, Traver D, Orkin SH. Expression of CD41 marks the initiation of definitive hematopoiesis in the mouse embryo. Blood. 2003;101:508-516.
25. Akashi K, Traver D, Miyamoto T, Weissman IL. A clonogenic common myeloid progenitor that gives rise to all myeloid lineages. Nature. 2000;404:193-197.
26. Kim I, He S, Yilmaz OH, Kiel MJ, Morrison SJ. Enhanced purification of fetal liver hematopoietic stem cells using SLAM family receptors. Blood. 2006;108:737-744.
27. Cumano A, Dieterlen-Lievre F, Godin I. Lymphoid potential, probed before circulation in mouse, is restricted to caudal intraembryonic splanchnopleura. Cell. 1996;86:907-916.
28. Medvinsky A, Dzierzak E. Definitive hematopoiesis is autonomously initiated by the AGM region. Cell. 1996;86:897-906.
29. de Bruijn MF, Ma X, Robin C, Ottersbach K, Sanchez MJ, Dzierzak E. Hematopoietic stem cells localize to the endothelial cell layer in the midgestation mouse aorta. Immunity. 2002;16:673-683.
30. Forsberg EC, Prohaska SS, Katzman S, Heffner GC, Stuart JM, Weissman IL. Differential expression of novel potential regulators in hematopoietic stem cells. PLoS Genet. 2005;1:e28.
31. Hirata Ki, Ishida T, Penta K, et al. Cloning of an immunoglobulin family adhesion molecule selectively expressed by endothelial cells. J Biol Chem. 2001;276:16223-16231.
32. Kincade PW, Owen JJ, Igarashi H, Kouro T, Yokota T, Rossi MI. Nature or nurture? Steady-state lymphocyte formation in adults does not recapitulate ontogeny. Immunol Rev. 2002;187:116-125.
33. Samokhvalov IM, Samokhvalova NI, Nishikawa SI. Cell tracing shows the contribution of the yolk sac to adult haematopoiesis. Nature. 2007;446:1056-1061.
34. Yao L, Yokota T, Xia L, Kincade PW, McEver RP. Bone marrow dysfunction in mice lacking the cytokine receptor gp130 in endothelial cells. Blood. 2005;106:4093-4101.
35. Wegmann F, Petri B, Khandoga AG, et al. ESAM supports neutrophil extravasation, activation of Rho, and VEGF-induced vascular permeability. J Exp Med. 2006;203:1671-1677.
36. Brass LF, Zhu L, Stalker TJ. Novel therapeutic targets at the platelet vascular interface. Arterioscler Thromb Vasc Biol. 2008;28[suppl]:S43-S50.
37. Zhang J, Niu C, Ye L, et al. Identification of the haematopoietic stem cell niche and control of the niche size. Nature. 2003;425:836-841.
38. Calvi LM, Adams GB, Weibrecht KW, et al. Osteoblastic cells regulate the haematopoietic stem cell niche. Nature. 2003;425:841-846.
39. Kiel MJ, Yilmaz OH, Iwashita T, Yilmaz OH, Terhorst C, Morrison SJ. SLAM family receptors distinguish hematopoietic stem and progenitor cells and reveal endothelial niches for stem cells. Cell. 2005;121:1109-1121.
40. Sugiyama T, Kohara H, Noda M, Nagasawa T. Maintenance of the hematopoietic stem cell pool by CXCL12-CXCR4 chemokine signaling in bone marrow stromal cell niches. Immunity. 2006;25:977-988.
41. Yin T, Li L. The stem cell niches in bone. J Clin Invest. 2006;116:1195-1201.
42. Orford KW, Scadden DT. Deconstructing stem cell self-renewal: genetic insights into cell-cycle regulation. Nat Rev Genet. 2008;9:115-128.
43. Balazs AB, Fabian AJ, Esmon CT, Mulligan RC. Endothelial protein C receptor (CD201) explicitly identifies hematopoietic stem cells in murine bone marrow. Blood. 2006;107:2317-2321.
44. Jokubaitis VJ, Sinka L, Driessen R, et al. Angiotensin-converting enzyme (CD143) marks hematopoietic stem cells in human embryonic, fetal, and adult hematopoietic tissues. Blood. 2008;111:4055-4063.
45. Massberg S, Schaerli P, Knezevic-Maramica I, et al. Immunosurveillance by hematopoietic progenitor cells trafficking through blood, lymph, and peripheral tissues. Cell. 2007;131:994-1008.
46. Welner RS, Kincade PW. Stem cells on patrol. Cell. 2007;131:842-844.
47. Massberg S, Konrad I, Schürzinger K, et al. Platelets secrete stromal cell-derived factor 1alpha and recruit bone marrow-derived progenitor cells to arterial thrombi in vivo. J Exp Med. 2006;203:1221-1233.

THE JOURNAL OF BIOLOGICAL CHEMISTRY VOL. 284, NO. 12, pp. 7719–7732, March 20, 2009

FIP1L1-PDGFRα Imposes Eosinophil Lineage Commitment on Hematopoietic Stem/Progenitor Cells*

Received for publication, September 26, 2008, and in revised form, December 22, 2008 Published, JBC Papers in Press, January 14, 2009, DOI 10.1074/jbc.M807489200

Kentaro Fukushima[‡], Itaru Matsumura[‡], Sachiko Ezoe[‡§1], Masahiro Tokunaga[‡], Masato Yasumi[‡], Yusuke Satoh[‡], Hirohiko Shibayama[‡], Hirokazu Tanaka[‡], Atsushi Iwama[¶], and Yuzuru Kanakura[‡]

From the [‡]Department of Hematology and Oncology, Osaka University Graduate School of Medicine, 2-2, Yamada-oka, Suita, Osaka 565-0871, Japan, the [§]Medical Center of Translational Research, Osaka University Hospital, Suita, Osaka 565-0871, Japan, and [¶]Cellular and Molecular Medicine, Graduate School of Medicine, Chiba University, Chiba 260-8670, Japan

Although leukemogenic tyrosine kinases (LTKs) activate a common set of downstream molecules, the phenotypes of leukemia caused by LTKs are rather distinct. Here we report the molecular mechanism underlying the development of hypereosinophilic syndrome/chronic eosinophilic leukemia by FIP1L1-PDGFRα. When introduced into c-Kit^{high}Sca-1^{+}Lineage^{-} cells, FIP1L1-PDGFRα conferred cytokine-independent growth on these cells and enhanced their self-renewal, whereas it did not immortalize common myeloid progenitors in *in vitro* replating assays and transplantation assays. Importantly, FIP1L1-PDGFRα but not TEL-PDGFRβ enhanced the development of Gr-1^{+}IL-5Rα^{+} eosinophil progenitors from c-Kit^{high}Sca-1^{+}Lineage^{-} cells. FIP1L1-PDGFRα also promoted eosinophil development from common myeloid progenitors. Furthermore, when expressed in megakaryocyte/erythrocyte progenitors and common lymphoid progenitors, FIP1L1-PDGFRα not only inhibited differentiation toward erythroid cells, megakaryocytes, and B-lymphocytes but aberrantly developed eosinophil progenitors from megakaryocyte/erythrocyte progenitors and common lymphoid progenitors. As for the mechanism of FIP1L1-PDGFRα-induced eosinophil development, FIP1L1-PDGFRα was found to more intensely activate MEK1/2 and p38^{MAPK} than TEL-PDGFRβ. In addition, a MEK1/2 inhibitor and a p38^{MAPK} inhibitor suppressed FIP1L1-PDGFRα-promoted eosinophil development. Also, reverse transcription-PCR analysis revealed that FIP1L1-PDGFRα augmented the expression of *C/EBPα*, *GATA-1*, and *GATA-2*, whereas it hardly affected *PU.1* expression. In addition, short hairpin RNAs against *C/EBPα* and *GATA-2* and *GATA-3KRR*, which can act as a dominant-negative form over all GATA members, inhibited FIP1L1-PDGFRα-induced eosinophil development. Furthermore, FIP1L1-PDGFRα and its downstream Ras inhibited PU.1 activity in luciferase assays. Together, these results indicate that FIP1L1-PDGFRα enhances eosinophil development by modifying the expression and activity of lineage-specific transcription factors through Ras/MEK and p38^{MAPK} cascades.

During the last decade, it has become clear that hematopoietic growth factors regulate only growth and survival of hematopoietic cells, whereas lineage-specific transcription factors, such as GATA-1, GATA-3, PU.1, Pax-5, C/EBPα, and C/EBPϵ, crucially control the lineage commitment and lineage-specific differentiation. For example, granulocyte colony-stimulating factor signaling induced megakaryopoiesis in granulocyte colony-stimulating factor receptor-transgenic mice (1). Also, erythropoietin (EPO)[2] was found to promote terminal granulocytic differentiation in EPO receptor-transgenic mice. From these data, we speculated that signal transduction molecules activated by hematopoietic growth factors would not influence the lineage commitment of hematopoietic stem cells/progenitor cells (HSCs/HPCs) or subsequent lineage-specific differentiation (2). However, it has very recently been shown that the MEK/ERK pathway is involved in myeloid lineage commitment (3). Also, PKB (c-Akt) was shown to be involved in lineage decision during myelopoiesis (4). In addition, FLT3-activating mutations were proved to inhibit C/EBPα activity through ERK1/2-mediated phosphorylation (3, 5). These results suggest that signal transduction molecules activated by hematopoietic growth factors or their genetic mutations would not only promote growth and survival but also influence lineage commitment and subsequent differentiation of hematopoietic cells.

Activating mutations of the tyrosine kinases (TKs), such as c-Kit, platelet-derived growth factor receptor (PDGFR), FLT3, and c-ABL, are provoked by several mechanisms, including chromosomal translocations and various mutations involving their self-regulatory regions. These mutations are often involved in the pathogenesis of various types of hematologic malignancies. BCR-ABL is known to cause chronic myelogenous leukemia and acute lymphoblastic leukemia. Most patients with *PDGFRβ* rearrangement reveal common clinical

* This work was supported by grants from the Ministry of Education, Science, Sports, and Culture and Technology of Japan. The costs of publication of this article were defrayed in part by the payment of page charges. This article must therefore be hereby marked "*advertisement*" in accordance with 18 U.S.C. Section 1734 solely to indicate this fact.

[1] To whom correspondence should be addressed: Dept. of Hematology and Oncology, Osaka University Graduate School of Medicine, 2-2, Yamada-oka, Suita, Osaka 565-0871, Japan. Tel.: 81-6-6879-3871; Fax: 81-6-6879-3879; E-mail: sezoe@bldon.med.osaka-u.ac.jp.

[2] The abbreviations used are: EPO, erythropoietin; LTK, leukemogenic tyrosine kinase; PDGFRα, platelet-derived factor receptor α; PDGFRβ, platelet-derived factor receptor β; KSL, Lin^{-}Sca^{-}1^{hi}c-Kit^{hi} cell; CMP, common myeloid progenitor; CLP, common lymphoid progenitor; GMP, common granulocyte/monocyte progenitor; HSC, hematopoietic stem cell; HPC, hematopoietic progenitor cell; C/EBP, CCAAT/enhancer-binding protein; MPD, myeloproliferative disorder; TK, tyrosine kinase; AML, acute myeloid leukemia; MAPK, mitogen-activated protein kinase; STAT, signal transducers and activators of transcription; HES, hypereosinophilic syndrome; CEL, chronic eosinophilic leukemia; ERK, extracellular signal-regulated kinase; LSC, leukemic stem cell; MEP, megakaryocyte/erythroid progenitor; FACS, fluorescence-activated cell sorter; shRNA, short hairpin RNA; RT, reverse transcription; GFP, green fluorescent protein; MEK, mitogen-activated protein kinase/extracellular signal-regulated kinase kinase.

features resembling chronic myelogenous leukemia or choronic myelomonocytic leukemia. In contrast, *FLT3* mutations (ITD and point mutations in the TK domain) are primarily detectable in acute myeloid leukemia (AML) or myelodysplastic syndrome (6–8). Also, c-*KIT* mutations in the TK domain ($Asp^{816} \rightarrow$ Val, Tyr, Phe, or His) are found in patients with aggressive mastocytosis, myelodysplastic syndrome, and AML (9–15). Although these leukemogenic TKs (LTKs) activate a common set of downstream signaling molecules, such as Ras/MAPK, PI3-K/Akt/mTOR, and STATs, the mechanisms by which LTKs cause different disease phenotypes remain to be clarified.

FIP1L1-PDGFRα is a fusion gene, which was originally identified in the patients with hypereosinophilic syndrome (HES)/chronic eosinophilic leukemia (CEL) (16, 17). FIP1L1-PDGFRα fusion protein supports cytokine-independent growth and survival of hematopoietic cells as a constitutively active TK (16, 18–21). As for the downstream signaling molecules, FIP1L1-PDGFRα was shown to activate STAT5, phosphatidylinositol 3-kinase, and Ras/ERK pathways like other LTKs, such as BCR-ABL, TEL-ABL, TEL-JAK2, and TEL-PDGFRβ (18). In addition, Buitenhuis *et al.* (22) recently reported that activation of phosphatidylinositol 3-kinase, ERK1/2, and STAT5 is pivotal for FIP1L1/PDGFRα-induced myeloproliferation.

The concept of "cancer stem cell" has widely been recognized and validated in various types of cancers, including breast cancer, brain tumors, colon cancer, lung cancer, and malignant melanoma. This concept was originally established in AML as a "leukemic stem cell (LSC)" (23, 24). In this concept, LSCs are defined as specific leukemic cells that can cause leukemia when transplanted into NOD/SCID mice. In AML, although leukemic blasts often display relatively homogenous features, they are organized in a hierarchy. Among them, LSCs reveal the most immature $CD34^+CD38^-$ phenotype similar to normal HSCs, whereas several antigen expressions are different. LSCs, which account for only 0.2–1.0% of AML cells in the bone marrow (BM), have both abilities to self-renew and to produce restrictedly differentiated leukemia cells, thereby maintaining themselves and yielding leukemia cells composing the majority (23, 25, 26). It is still unclear whether LSCs originate solely from HSCs or are generated from nonstem immature cells that have acquired *de novo* self-renewal ability. It has been shown that, although common myeloid progenitors (CMPs) and granulocyte/monocyte progenitors (GMPs) have very limited life spans, several leukemogenic oncogenes, such as *MLL-ENL*, *MOZ-TIF2*, and *MLL-AF9*, have an ability to immortalize these cells, thereby enabling them to act as LSCs (27, 28). On the other hand, although LSCs in a chronic phase of chronic myelogenous leukemia are at an HSC level, chronic myelogenous leukemia cells at a CMP/GMP level can act as LSCs in an accelerated phase, suggesting that additional gene mutations can change the main LSC population during disease progression. From these findings, it is now speculated that the leukemia phenotype is determined by the biologic property of the mutated gene and/or the lineage and the differentiation state of LSCs.

In an attempt to analyze the molecular mechanisms by which each LTK causes leukemia with the specific phenotype, we introduced FIP1L1-PDGFRα, which plays a causal role in HES/CEL, into murine HSCs and various types of HPCs. As a result, we found that FIP1L1-PDGFRα specifically enhanced eosinophil development from HSCs/HPCs and imposed the lineage conversion to eosinophil lineage on megakaryocyte/erythroid progenitors (MEPs) and common lymphoid progenitors (CLPs) through Ras/MEK and $p38^{MAPK}$ cascades by modifying the expression and activity of lineage-specific transcription factors.

EXPERIMENTAL PROCEDURES

Reagents and Antibodies—Recombinant human TPO was provided by Kirin Brewery (Tokyo, Japan). Recombinant human FLT3L, human IL-6, murine SCF, murine IL-5, murine IL-7, murine granulocyte-macrophage colony-stimulating factor, and human EPO were purchased from Peprotech (Hamburg, Germany).

Antibodies, Cell Staining, and Sorting—To isolate KSLs and CLPs, murine BM cells were stained with phycoerythrin-conjugated anti-IL-7Rα chain (SB/199) (eBioscience, San Diego, CA), fluorescein isothiocyanate-conjugated anti-Sca-1 (E13-161-7), and APC-conjugated anti-c-Kit (2B8) monoclonal antibodies, and biotinylated rat antibodies specific for the lineage markers Ter119, CD3ε (145-2C11), B220 (RA3–6B2), and Gr-1 (RB6-8C5), followed by staining with streptavidin-PerCP/Cy5.5 (BD Biosciences). Then KSLs and CLPs were sorted as $IL\text{-}7R\alpha^-Lin^-Sca\text{-}1^{hi}c\text{-}Kit^{hi}$ and $IL\text{-}7R\alpha^+Lin^-Sca\text{-}1^{lo}c\text{-}Kit^{lo}$ populations, respectively. For myeloid progenitor sorting, murine BM cells were stained with phycoerythrin-conjugated anti-FcγRII/III (2.4G2), fluorescein isothiocyanate-conjugated anti-CD34 (RAM34) (BD Biosciences), APC-conjugated anti-c-Kit, biotinylated anti-Sca-1, and anti-IL-7Rα (SB/199) (Serotec, Raleigh, NC) monoclonal antibodies, and the above described lineage mixture of monoclonal antibodies (BD Biosciences), followed by staining with avidin-APC/Cy7 (BD Biosciences). After the staining, $IL\text{-}7R\alpha^-Lin^-Sca\text{-}1^-c\text{-}Kit^+CD34^+Fc\gamma RII/III^{lo}$ were sorted as CMPs, $IL\text{-}7R\alpha^-Lin^-Sca\text{-}1^-c\text{-}Kit^+CD34^+Fc\gamma RII/III^{hi}$ as GMPs, and $IL\text{-}7R\alpha^-Lin^-Sca\text{-}1^-c\text{-}Kit^+CD34^-Fc\gamma RII/III^{lo}$ as MEPs, as described previously (29). All of these HSCs and HPCs were isolated using a FACS Aria (BD Bioscience, San Jose, CA). In all analyses and sorting, dead cells were excluded by staining with 7-amino-actinomycin D (Calbiochem). Cells were stained with phycoerythrin-conjugated CD125 (IL-5 receptor α-subunit, T21) and APC-conjugated Gr-1(RB6–8C5) (BD Biosciences) for detection of eosinophil lineage.

Plasmids—Expression vectors for FIP1L1-PDGFRα and TEL-PDGFRβ were kindly provided by Dr. D. Gary Gilliland (Harvard Medical School, Boston, MA). Expression vectors for PDGFRα V561D and D842V were kindly provided by Dr. S. Hirota (Hyogo Medical School, Hyogo, Japan). *FIP1L1-PDGFRα*, *TEL-PDGFRβ*, *PDGFRαV561D*, and *PDGFRαD842V* were cloned into the murine stem cell virus-internal ribosome entry site-EGFP (pMie) vector. Also, we constructed *FIP1L1-PDGFRβ* and *TEL-PDGFRα* by the PCR method and subcloned them into pMie.

Short hairpin RNA (shRNA) interference oligonucleotides against GATA-2 and C/EBPα described previously (30, 31) were cloned into an shRNA expression vector, pCS-RfA-CG, which was kindly provided by Dr. Miyoshi H (RIKEN Bio-

Resource center, Tsukuba, Japan). The retrovirus expression vector for dominant negative GATA was constructed by cloning human *GATA-3KRR* cDNA that can inhibit GATA-1, GATA-2, and GATA-3 (32) into pMie.

Cell Culture and Preparation—Murine BM cells were obtained from 6–8-week-old C57BL/6J mice, which were purchased from CLEA (Tokyo, Japan). After sedimentation of the red blood cells with 6% hydroxyethyl starch, mononuclear cells were separated by density gradient centrifugation, using HISTOPAQUE 1083 (Sigma). KSLs, CMPs, GMPs, and MEPs were purified from mononuclear cells and cultured in RPMI1641 medium (Nacalai Tesque, Kyoto, Japan) supplemented with 10% fetal calf serum (EQUITECH-BIO, Kerrville, TX) in the presence of murine SCF (50 ng/ml), human FLT3L (10 ng/ml), human IL-6 (50 ng/ml), and human TPO (50 ng/ml) for 48 h, and the cells were subjected to the retrovirus infection.

Retrovirus Transduction—The conditioned media containing high titer retrovirus particles were prepared as described previously (33). Briefly, an ecotropic packaging cell line, 293gp, kindly provided by Dr. H. Miyoshi (RIKEN BioResource Center, Tsukuba, Japan), was transfected with each retrovirus vector by the calcium phosphate coprecipitation method. After 12 h, the cells were washed and cultured for 48 h. To produce lentivirus, 293T cells were transfected with each shRNA expression vector together with a packaging vector (pCAG-HIVgp) and a lentivirus envelope and Rev construct (pCMV-VSV-G-RSV-Rev), both of which were provided by Dr. Miyoshi. Then the supernatant containing virus particles was collected, centrifuged, and concentrated 50-fold in volume. The precultured murine BM cells were infected with each retrovirus in the RPMI1641 medium supplemented with the same medium containing protamine sulfate for 48 h in 6-well dishes coated with RetroNectin (Takara Bio Inc., Shiga, Japan).

Colony Assays—Cells were seeded into methylcellulose medium (MethoCult GF M3434; Stem Cell Technologies, Vancouver, Canada) at a density 2.5×10^2 cells/35-mm dish and were cultured with 5% CO_2 at 37 °C. All cultures were performed in triplicate, and the numbers of colonies were counted after 10 days.

In Vitro Immortalization Assays for HPCs—Immortalization assays of HPCs *in vitro* were performed as previously described (34). In brief, 10^4 cells were plated in 1.1 ml of methylcellulose medium (Methocult M3434). After the 1 week of culture, colony numbers were counted, and single-cell suspensions of colonies (10^4 cells) were subsequently replated under identical conditions. Replating was repeated every week in the same way.

Luciferase Assays—Luciferase assays were performed with a dual luciferase reporter system (Promega, Madison, WI), as previously described (35). Briefly, 293T or NIH3T3 cells (2×10^5 cells) were seeded in a 60-mm dish and cultured for 24 h. Using the calcium phosphate coprecipitation method, cells were transfected with 2 μg of reporter gene (pGL3-3×MαP-luciferase, 3×MHC-luciferase, or 1×MPO-luciferase) in combination with 2 μg of pcDNA3-GATA1, pcDNA3-PU.1 (36), or pcDNA3-C/EBPα together with 6 μg of an empty vector or an effector vector for FIP1L1-PDGFRα, H-RasG12V, 1*6-STAT5A (37), or CAAX-p110 (38) and 10 ng of pRL-CMV, a *Renilla* luciferase expression vector. After 12 h, cells were washed, serum-starved for 24 h, and subjected to luciferase assays. After 36 h, the cells were lysed and subjected to a measurement for luciferase activity. The relative firefly luciferase activity was calculated by normalizing transfection efficiency according to the *Renilla* luciferase activity.

Semiquantitative RT-PCR Analysis—Total RNA was isolated from 5×10^4 FACS-sorted GFP-positive cells using TRIzol reagent (Invitrogen). RT-PCR was performed using SuperScript II reverse transcriptase (Invitrogen) according to the manufacturer's instructions. The cDNA product (1 μl) was resuspended in 20 μl of the PCR buffer containing 0.5 units of TaqGold DNA polymerase (PerkinElmer Life Sciences), 2 mM $MgCl_2$, and 15 pmol of forward and reverse primers. The sequences of forward/reverse primer sets were as follows: *C/EBPα*, 5′-GCC TGG CCT TGA CCA AGG AG-3′ and 5′-CAC AGG ACT AGA ACA CCT GC-3′; *GATA-1*, 5′-GGA ATT CGG GCC CCT TGT GAG GCC AGA GAG-3′ and 5′-CGG GGT ACC TCA CGC TCC AGC CAG ATT CGA CCC-3′; *GATA-2*, 5′-CGG AAT TCG ACA CAC CAC CCG ATA CCC ACC TAT-3′ and 5′-CGG AAT TCG CCT ACG CCA TGG CAG TCA CCA TGC T-3′; *IL5-Rα*, 5′-GCC CTT TGA TCA GCT GTT CAG TCC AC-3′ and 5′-CGG AAC CGG TGG AAA CAA CCT GGT C-3′; *MBP*, 5′-ACC TGT CGC TAC CTC CTA-3′ and 5′-GTG GTG GCA GAT GTG TGA-3′; *PU.1*, 5′-GAT GGA GAA AGC CAT AGC GA-3′ and 5′- TTG TGC TTG GAC GAG AAC TG-3′; *HPRT*, 5′-CAC AGG ACT AGA ACA CCT GC-3′ and 5′-GCT GGT GAA AAG GAC CTC T-3′.

The PCR products were electrophoresed in agarose gels containing ethidium bromide, and their amounts were analyzed with a Fluor Imager595 and ImageQuant software (Amersham Biosciences).

Transplantation Assays—Transplantation assays were performed according to procedures described previously (39). Briefly, 8–12-week-old CD45.2 mice were lethally irradiated (900 rads) 24 h before the transplantation. BM cells isolated from congenic C57BL/6 (B6-Ly5.1) mice were transduced with FIP1L1-PDGFRα, and 10,000 GFP-positive cells were injected intravenously in combination with 2×10^5 normal BM cells with CD45.2 phenotype. Chimeric analyses were performed at 4 weeks and 8 weeks, and mice were sacrificed 16 weeks after transplantation. Animal care was performed according to institutional guidelines.

Measurement of Phosphorylation of Intracellular Signaling Molecules—Phosphorylation of intracellular molecules was assessed using Phosflow technology (BD Biosciences) according to the manufacturer's recommendation. Briefly, cells were fixed with Phosflow Fix Buffer and incubated at 37 °C for 10–15 min. After permeabilization at room temperature for 10 min, cells were washed twice with Phosflow Perm/Wash Buffer and incubated at room temperature for 10 min. After the binding reaction to each antibody, cells were washed once with Phosflow Perm/Wash buffer, resuspended in 500 μl of BD Pharmingen stain buffer (BD Bioscience), and then subjected to flow cytometric analysis. All experiments were repeated independently at least three times, and reproducibility was confirmed.

Statistical Analyses—Statistical analyses were performed using Student's *t* test.

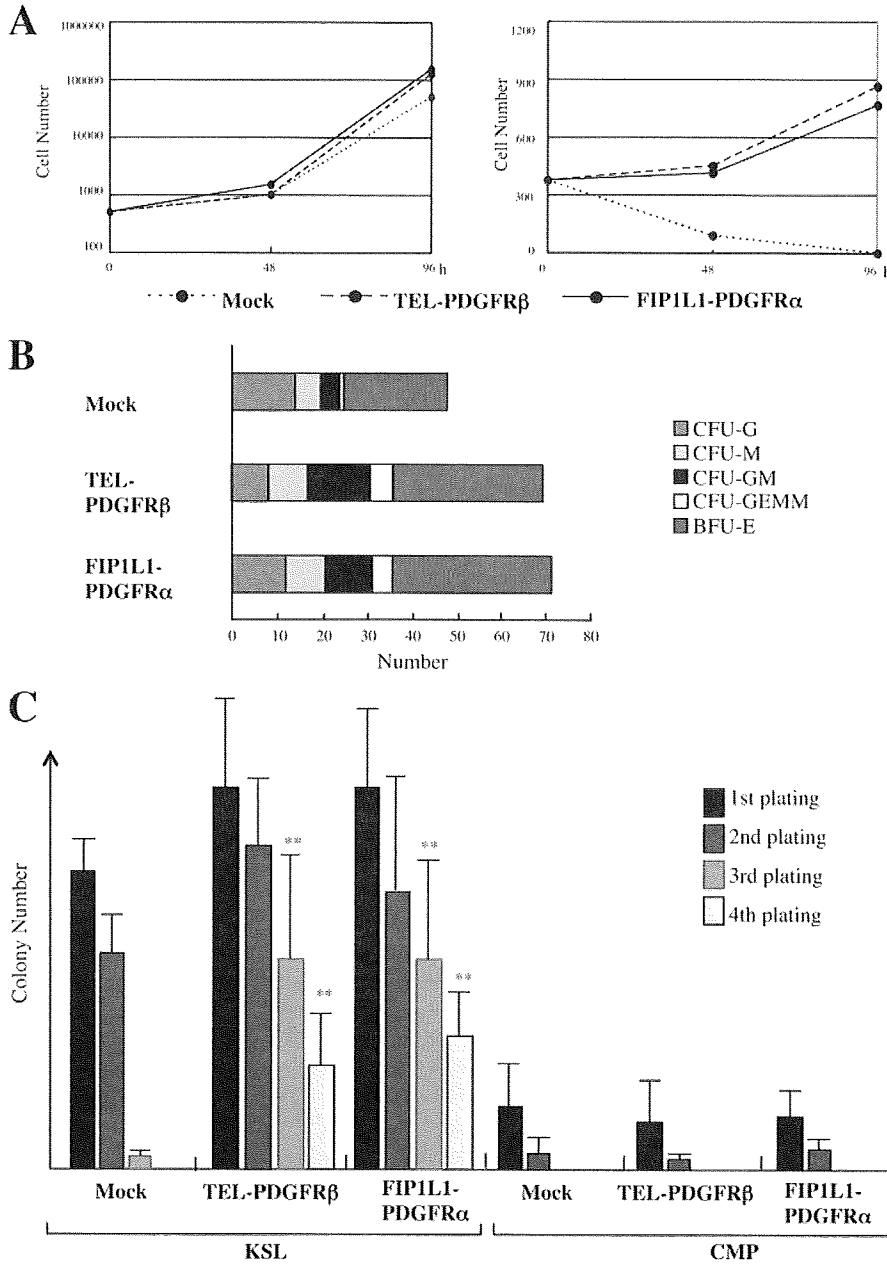

FIGURE 1. **The effects of leukemogenic tyrosine kinases on proliferation and survival of hematopoietic stem/progenitor cells.** *A*, KSLs were isolated from murine bone marrow mononuclear cells. After the retrovirus (mock, FIP1L1-PDGFRα, or TEL-PDGFRβ) infection, retrovirus-infected KSLs were sorted as GFP^+ cells and cultured with (*left*) or without (*right*) SCF, TPO, FLT3L, and IL-6 for 96 h. During these cultures, total viable cell numbers were counted at the time indicated. *B*, KSLs infected with each retrovirus were sorted and seeded into the methylcellulose medium containing EPO, TPO, SCF, granulocyte colony-stimulating factor, and IL-3. Colony numbers were counted on day 12. *C*, immortalization assays for retrovirus-infected KSLs and CMPs. Retrovirus-infected KSLs and CMPs (10^3 cells) were plated into methylcellulose medium, and colony numbers were counted after 1 week. Then single-cell suspensions of colonies (10^3 cells) were serially replated every week in the same way. *Bars*, number of colonies obtained after each round of replating in methylcellulose as means ± S.D. ($n = 3$). **, $p < 0.01$ compared with the value of mock-transduced cells.

RESULTS

Effects of FIP1L1-PDGFRα on the Growth and Survival of Murine KSL Cells—To investigate the effects of LTKs on the growth, differentiation, and survival of HSCs/HPCs, we constructed bicistronic retrovirus vectors for FIP1L1-PDGFRα and TEL-PDGFRβ, which express these cDNAs together with EGFP through the internal ribosome entry site in the infected cells. At first, we introduced these retrovirus vectors into KSL cells. After a 48-h infection, 55–65% of KSLs were found to be GFP-positive in all of transfectants by flow cytometric analysis (data not shown). Next, we isolated retrovirus-infected cells as GFP-positive cells and cultured them in the medium with or without SCF, TPO, FLT3L, and IL-6. As shown in Fig. 1*A* (*left*), neither FIP1L1-PDGFRα nor TEL-PDGFRβ further augmented cytokine-dependent growth of KSLs. However, these LTKs enabled KSLs to survive and proliferate under cytokine-deprived conditions at least for 96 h, whereas mock (an empty retrovirus)-infected KSLs rapidly led to apoptosis in this condition (Fig. 1*A*, *right*).

Next, we performed colony assays using these retrovirus-infected KSLs. After 2-day retrovirus infection, GFP-positive cells were sorted and plated into methylcellulose medium containing the cytokine mixture (EPO, TPO, SCF, granulocyte colony-stimulating factor, and IL-3), and numbers of colonies were counted after 10 days. As shown in Fig. 1*B*, the total number of colonies that developed from FIP1L1-PDGFRα- or TEL-PDGFRβ-infected KSLs was increased by 40–50% as compared with that from mock-infected KSLs. Also, these colonies were larger than those yielded from mock-infected KSLs (data not shown). However, the proportion of CFU-GEMM, CFU-GM, CFU-G, CFU-M, and BFU-E was roughly the same among three transfectants, indicating that these LTKs scarcely influence the lineage commitment and differentiation of KSLs in colony assays performed in this cytokine combination (Fig. 1*B*).

We next performed an *in vitro* immortalization assay using FIP1L1-PDGFRα-, TEL-PDGFRβ-, or mock-transduced KSLs and CMPs. After the first and second plating, both FIP1L1-PDGFRα- and TEL-PDGFRβ-transduced KSLs yielded a slightly increased number of colonies relative to mock-transduced KSLs, whereas these differences were not significant (Fig. 1*C*, *left*). Also, in contrast to mock-transduced KSLs, FIP1L1-PDGFRα- or TEL-PDGFRβ-transduced KSLs